

Simulation of a High-Redshift Line-Emitting Galaxy Detection with DESHIMA using TiEMPO

Yannick Roelvink

Delft University of Technology

SIMULATION OF A HIGH-REDSHIFT LINE-EMITTING GALAXY DETECTION WITH DESHIMA USING TIEMPO

by

Yannick Roelvink

in partial fulfillment of the requirements for the degree of

Bachelor of Science
in Applied Physics

at the Delft University of Technology,
to be defended publicly on the 17th of August 2020, 13:00

Supervisor:	Dr. A. Endo,	TU Delft
Thesis committee:	Dr. A. J. L. Adam,	TU Delft
	Dr. S. J. C. Yates,	SRON

This thesis is confidential and cannot be made public until 17 August 2020

Credits of the front page picture:
ASTE Telescope: Akira Endo

An electronic version of this thesis is available at <http://repository.tudelft.nl/>.

ABSTRACT

In this report, we will focus on simulating galaxy observations with the Deep Spectroscopic High-redshift Mapper (DESHIMA). To do so, we will discuss and evaluate two main parts needed to accurately perform such a simulation:

Firstly, we will answer the question whether Time-dependent End-to-end Model for Post-process Optimization (TiEMPO)[1], the modelling software used for DESHIMA observation simulations, is able to accurately simulate real life galaxy observations conditions. To do so, the simulation program is fed artificially created atmospheric data and its output is compared with sky brightness data of real measurements. More specifically, the time signal, power spectral density and noise equivalent flux density of both the simulation and the measurement data are derived and compared. This comparison showed, apart from a linear drift of the time signal data and a small offset of the power spectral density, good agreement between the simulation and the measurement.

The second part of this thesis discusses whether we can detect an artificially created galaxy, using the already verified atmospheric model of TiEMPO. To do so, the output of the simulation is run through a series of algorithms that calculate the observation spectrum of the telescope, as if it were a real measurement. In addition, the application of different observation tactics and telescope parameters are tested and visualised. Most importantly, two observational position-switching (chopping) techniques are applied and compared: the dual point and ABBA chopping techniques. To test the effectiveness of the two chopping techniques, both will be used to simulate atmospheric filtration using stationary, i.e. without telescope movement, simulation and measurement data, which do not contain the (to be detected) galactic data. As there is no telescope movement, nor galactic data, the spectra should ideally fluctuate around zero. However, as we will see in this report, this is not obtained in all cases. After further analysis, two main types of offsets could be identified: the first one originating from the linear drift of the measurement's time signal data, whereas the second one is due to the spatial displacement of the chopping positions. The former can be corrected by applying the ABBA chopping technique rather than the dual chopping method, whereas the latter cannot with either of the two.

Using the insights we acquire from running these simulations with observation conditions for DESHIMA, we are able to perform an actual galaxy observation simulation. The galactic data acquired from this observation simulation shows good agreement with the input values of the galaxy data of TiEMPO, assuring that TiEMPO can be used for galaxy observation simulations.

CONTENTS

List of Symbols	1
1 Introduction	3
2 Properties of Ground-Based Galaxy Observations	5
2.1 Emission Spectra	5
2.1.1 Redshift	5
2.2 Atmospheric Influence	6
2.2.1 ARIS	7
3 Verification of TiEMPO	9
3.1 Sky Temperature	9
3.2 Power Spectral Density	10
3.2.1 Flux Density	10
3.2.2 Power Density	11
3.2.3 Simulation versus Measurement	12
3.3 Noise-Equivalent Flux Density	14
4 Observation Simulations	17
4.1 Sky Chopping	17
4.2 Dual Chopping	20
4.2.1 Effects of Atmospheric Changes	20
4.3 ABBA Chopping	21
4.3.1 Measurement vs TiEMPO	23
4.4 Choice of Chopping Method	24
4.4.1 DESHIMA 1.0	25
4.4.2 DESHIMA 2.0	26
4.5 DESHIMA 2.0 Galaxy Observation Simulation	28
5 Conclusions and Future Work	31
5.1 Conclusions	31
5.2 Future Work	32
Appendices	33
A: Overview of TiEMPO	33
B: Used TiEMPO Parameters	34
C: TiEMPO data without added atmospheric drift	35
D: Project Output	39
Acknowledgements	41
Bibliography	43

LIST OF SYMBOLS

Abbreviations

ARIS	Astronomical Radio Interferometer Simulator
ASTE	Atacama Submillimetre Telescope Experiment
DESHIMA	Deep Spectroscopic High-Redshift Mapper
DSFG	Dusty Star-Forming galaxy
SMG	Submillimetre-Bright Galaxy
TiEMPO	Time-dependent End-to-end Model for Post-process Optimization

Physical Constants

h	Planck's constant	$6.62607004 \cdot 10^{-34} \text{ m}^2 \text{ kg s}^{-1} \text{ Hz}^{-1}$
k	Boltzmann's constant	$1.38064852 \cdot 10^{-23} \text{ m}^2 \text{ kg , s}^{-2} \text{ K}^{-1}$

Parameters

η_{atm}	Atmospheric Transmission Coefficient	
η_{MB}	Main Beam Efficiency	
λ	Wavelength	m
Ω_{MB}	Solid Angle of Main Beam	sr
A_e	Effective Aperture Area	m^2
EPL	Extra Path Length	m
F	Frequency	Hz
F_v	Flux density	Jy or $\text{W m}^{-2} \text{ Hz}^{-1}$
n	Ratio of nodding and chopping frequencies of ABBA	
$NEFD$	Noise-Equivalent Flux Density	$\text{Jy s}^{0.5} \text{ beam}^{-1}$
P_v	Power Density	W Hz^{-1}
psd_F	Flux-based Power spectral density	$\text{Jy}^2 \text{ Hz}^{-1}$
psd_T	Temperature-based Power spectral density	$\text{K}^2 \text{ Hz}^{-1}$
pwv	Precipitable water vapour	m
S_F	Flat level of Flux-based Power Spectral Density	$\text{Jy}^2 \text{ Hz}^{-1}$
T	(Sky) Temperature	K
z	Redshift	

1

INTRODUCTION

Over the years, astronomers have been able to observe more and more distant star systems and galaxies. Equipped with highly advanced optical measurement tools, their telescopes are looking far into the cosmos, collecting immense amounts of data about the history of the universe. These observation campaigns have established the importance of dusty galaxies for star formation in the (early) universe [2]. The clouds of dust and gas surrounding these Dusty Star-Forming galaxies (DSFGs) absorb most of the emitted optical radiation, which is re-emitted as infrared radiation again by the dust itself [3]. Due to this absorption and re-emission, DSFGs are often very faint within the optical spectrum, whereas they shine brightly in the infrared spectrum. Observing these bright infrared dusty galaxies, also called Submillimetre-Bright Galaxies (SMGs), imposes its own difficulties, as all objects in the universe emit some level of infrared radiation, which adds additional noise to the observation data. The most dominant source of noise is the Earth's atmosphere, as its attenuation and re-emission of infrared light greatly affects ground-based telescope observations.

That is where the Dutch-Japanese Deep Spectroscopic High-redshift Mapper, or DESHIMA for short, comes into view. This revolutionary submillimetre spectrometer can observe these dusty galaxies with a previously unknown frequency bandwidth. This superconducting chip has been developed to determine the redshift of extragalactic objects, which in turn tells us about both the distance to and the age of the observed galaxy. It does this by using 49 detection channels, each tuned to a different frequency, while being placed inside the Atacama Submillimetre Telescope Experiment (ASTE) telescope in the Atacama Desert, Chile. Since its first light in 2017, it has successfully performed a range of test procedures and measurements. With these tests, the DESHIMA research team has proven that, with some improvements, it is possible to detect DSFGs with this type of spectrometer [4] [5].

In 2020, they aim to install their improved version of the spectrometer, called DESHIMA 2.0, onto ASTE. It will have an extended range of observable frequencies, ranging from 220–440 GHz, split up into 347 detection channels. With this significant improvement of bandwidth, there are high hopes that DESHIMA 2.0 will be able to observe much fainter galaxies than its predecessor.

Being able to observe very faint galaxies is a remarkable achievement on its own, but putting it to practise is easier said than done: Questions like where to point the telescope, how to observe the galaxy and how to filter out all the interference sources are preferably discussed and solved before commencing on the scarce research campaigns. Precisely because of this reason, the Time-dependent End-to-end Model for Post-process Optimization (TiEMPO) was created [1]. It enables the DESHIMA research team to simulate and test their observation tactics before performing them with the telescope. However, to do so, one must be certain that TiEMPO simulates the observations accurately, and that the observation tactics can be simulated in the first place.

This thesis will therefore focus on two important parts: Firstly, it will analyse the used end-to-end model, TiEMPO, and check whether this model accurately simulates real-world situations. As stated before, Earth's atmosphere is the most prominent source that adds noise to the galactic radiation. In addition, the atmospheric transmission and absorption rates are highly non-linear in the 220–440 GHz observation range of the DESHIMA 2.0 spectrometer, making it complex to remove this noise. A proper verification of TiEMPO is therefore crucial: By comparing various aspects of both simulated and measured atmospheric data, the accuracy of TiEMPO will be assessed and evaluated, eventually leading to the conclusion whether or not TiEMPO can be accepted as a proper end-to-end model of atmospheric observations.

In addition, galaxy observation techniques will be simulated with simulation parameters similar as those used during DESHIMA 1.0 observations. Comparing the output of these TiEMPO observation simulations with the measurement data provides us with the final test whether TiEMPO can accurately be used for DESHIMA simulations.

Finally, TiEMPO will be used to simulate DESHIMA 2.0 observations. As these observations have yet to be performed, the conclusions acquired from these simulations will be used to give the first recommendations for the DESHIMA 2.0 observation campaign obtained via TiEMPO.

2

PROPERTIES OF GROUND-BASED GALAXY OBSERVATIONS

In this first chapter, we will take a look at some of the physical phenomena TiEMPO has to consider for proper ground-based galaxy observation simulations. More specifically, we will follow the path of radiation emitted by Submillimetre-Bright Galaxies (SMGs) all the way to detection with a spectrometer and observe which influence each of the parts of its journey have. We will then discuss briefly how these influences are incorporated in TiEMPO.¹

2.1. EMISSION SPECTRA

Starting from galaxy, two main types of emission can be observed:

Firstly, we have the so-called continuum emission. This type of emission is emitted by large constructions of atoms, such as stellar cores. Together, these large constructions create a wide and continuous spectrum of radiation. For most SMGs it is the case that their continuum emission is (partially) absorbed by the gas and dust particles surrounding them. The part of the continuum emission that is still detectable are often used to find new SMGs with continuum cameras. It is, however, inaccurate to measure the redshift of an SMG with only its continuum emission spectrum.

The other type of emission is the so-called line emission: Because of transitions within their fine structure energy levels, atoms and molecules can emit photons with very specific wavelengths. These transitions occur, for example, in the gas and dust particles surrounding SMGs, which absorb the continuous radiation emitted by the galaxy itself. The radiation emitted by the surrounding gas that de-excites back after absorbing the galaxies radiation can afterwards be detected and analysed from Earth. One of the most well-known emissions lines used within astronomy is that of singly ionised carbon atoms (C^+), also known as the [CII] line [6].

2.1.1. REDSHIFT

DESHIMA's main goal is to detect the redshift of galaxies, i.e. the increase of wavelength of its emission spectrum due to an increase in distance between source and observer. In astronomy, the amount of redshift of an object is denoted with the letter z and mathematically defined as [7]

¹A full overview of the TiEMPO model can be found in Appendix A

$$1 + z = \frac{\lambda_{\text{obs}}}{\lambda_{\text{emit}}} = \frac{F_{\text{emit}}}{F_{\text{obs}}} \quad (2.1)$$

where λ_{obs} and F_{obs} indicate the wavelength and frequency of the observed and λ_{emit} and F_{emit} the wavelength and frequency of the emitted radiation are. But how do we know at which frequency (or wavelength) the radiation was emitted from the galaxy?

That is where the line emissions come into place: emission lines occur on very specific frequencies, their so-called *rest frequencies* (F_{rest}). Due to the fact that these rest frequencies are constant, the observed frequency lines can easily be compared with the rest frequency of an emission line. For example, the rest frequency of the previously mentioned [CII] line is 1901 GHz [8].

2.2. ATMOSPHERIC INFLUENCE

When the radiation consisting of these emission lines reaches the Earth, it has not reached the telescope yet. In order to do that, the radiation has to pass through Earth's atmosphere, which interferes with the radiation.

There are two ways in which Earth's atmosphere interferes with the galaxy emission radiation: Attenuation and re-emission[6][9]. Similar to the dust around the SMGs, Earth's atmosphere consists of atoms that can be excited by an external energy source. when the radiation originating from the observed galaxy reaches these atoms, they can absorb some of its energy. This process is called atmospheric attenuation and lowers the amount of available radiation for detection. In addition, the atmosphere itself is a radiating body, emitting energy multiple times that of the galactic source. This non-galactic data is then also observed by the telescope, literally clouding the much fainter galactic data. An illustration of this is given in Figure 2.1.

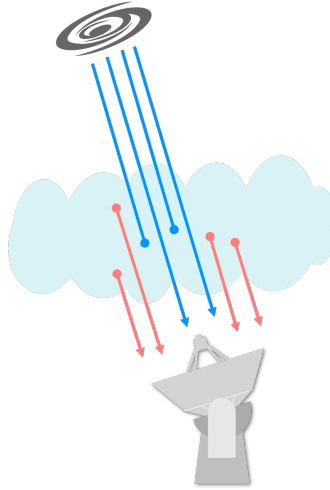


Figure 2.1: A visualisation of atmospheric interference with galactic data, obtained from [6]. The blue lines illustrate the attenuation of the atmosphere, whereas the red lines illustrate the re-emission.

However, the attenuation rate is dependent on the frequency of the galactic signal. This frequency-dependency is commonly visualised using the so-called *atmospheric transmission coefficient* (η_{atm}), where the transmission rate is the percentage of the total signal that is not attenuated. When plotting η_{atm} over a range of frequencies, a plot like in Figure 2.2 is observed.

However, that is not all: Even when the galactic signal manages to get through Earth's atmosphere, it will still be influenced by its opacity. As it turns out, the Precipitable Water Vapour (*pwv*), i.e. the height of the water column obtained if all the water vapour in the atmosphere were precipitated as rain, has a direct correlation with the Extra Path Length (*EPL*), i.e. the increase in optical path length [1] [12].

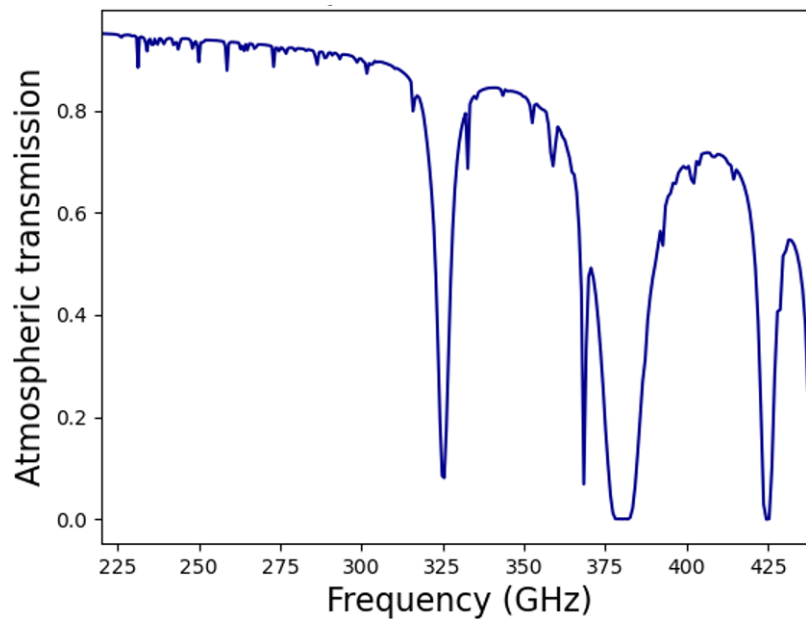


Figure 2.2: Plot of the atmospheric transmission coefficient over a range of frequencies. The atmospheric transmission coefficient is defined as the percentage of the total data that is not attenuated, so higher values indicate less atmospheric interference. Figure obtained from [1], data for figure acquired from [10] and [11].

2.2.1. ARIS

In order to accurately simulate the atmosphere’s influence on the galaxy’s emission spectra, TiEMPO uses a tool that simulates the consistency of Earth’s atmosphere over the span of an entire observation: The Astronomical Radio Interferometer Simulator, or ARIS for short [13] [14]. This atmospheric simulation device takes input arguments such as the Root-Mean Square (RMS) value of the *EPL* for a certain distance and the structure factor of the atmosphere into account and creates a 2D simulated map of *EPL* data of the atmosphere. Converting the *EPL* into *p_{wv}* using the relation found in [1] results into a plot similar to that in Figure 2.3.²

When observing only the *EPL* and *p_{wv}* data from a single vertical position of the simulation, a plot like Figure 2.4 is obtained. Because we plot only the data from a single simulation position, the temporal fluctuations have been converted into spatial fluctuations because of the presence of the wind.

Using ARIS, TiEMPO assumes that all atmospheric noise originates from the *p_{wv}* fluctuations, as observed in Figure 2.4. As a matter of fact, Yashoda Sewnarain Sukul discovered that fluctuations in the observed sky data made with DESHIMA are indeed mainly caused by these fluctuations [15]. This justifies the assumption made earlier and ensures that TiEMPO can use the data from ARIS safely.

²Note that Figure 2.3 is a static frame from a moving simulation. For an animation of the ARIS simulation, use the following qrcode:



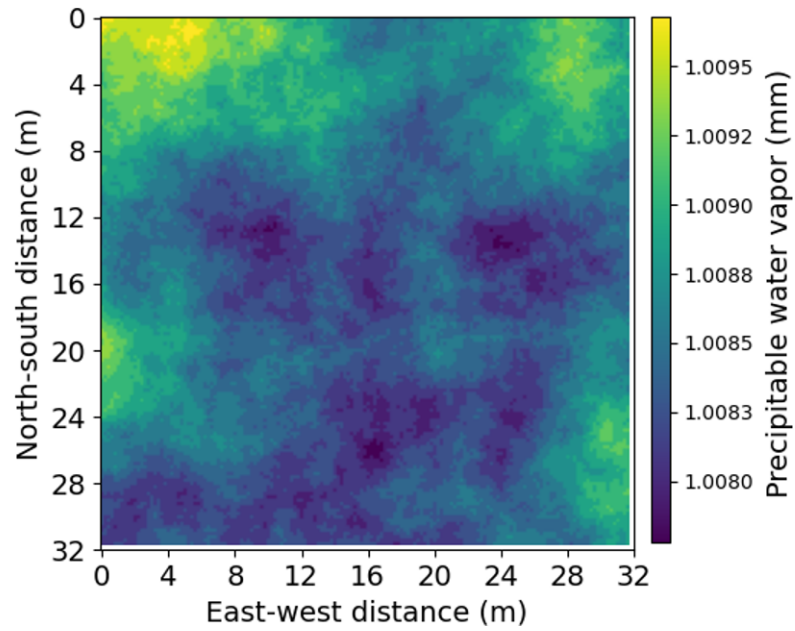


Figure 2.3: A 2D colour map of a simulated atmosphere, acquired via The Astronomical Radio Interferometer Simulator (ARIS). The colours in the plot indicate the level of pww at each individual pixel. Obtained from [1]

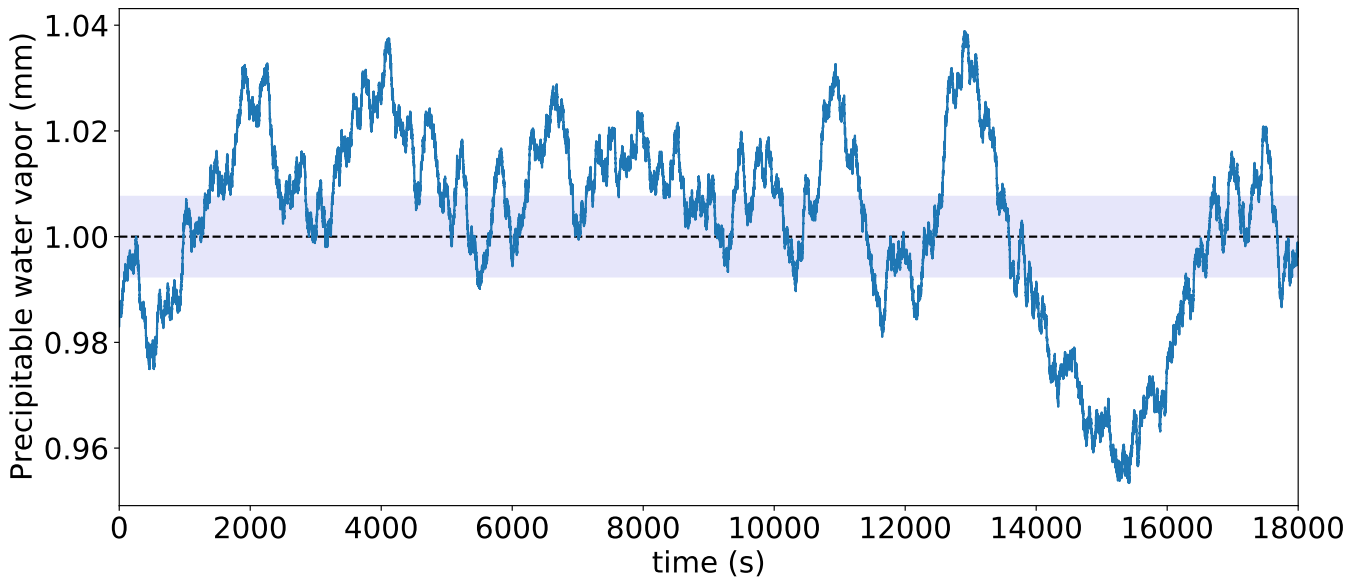


Figure 2.4: Data of the ARIS simulated atmosphere, but from only a single vertical position over time. The average value pww , which was in all the simulations used in this paper set to 1 mm, is indicated with the black line. The grey area indicates the area in which the pww value is within one standard deviation of the average value. Obtained from [1]

3

VERIFICATION OF TIEMPO

In order to verify the accuracy of the atmospheric model used within TiEMPO, 3 aspects of the output of the simulation are compared with those of the raw atmospheric measurement data, acquired with the DESHIMA 1.0 spectrometer. To do so accurately, TiEMPO will be run with DESHIMA 1.0 parameters.¹

3.1. SKY TEMPERATURE

Firstly, the raw sky temperature (T_{sky}) data from the DESHIMA observation is compared with TiEMPO's output with similar parameters. The final plot acquired is shown in Figure 3.1, where the blue plot the measurement and the orange plot the simulation data are. For both the measurement and simulation data in Figure 3.1, the data is taken from the 350 GHz spectrometer.

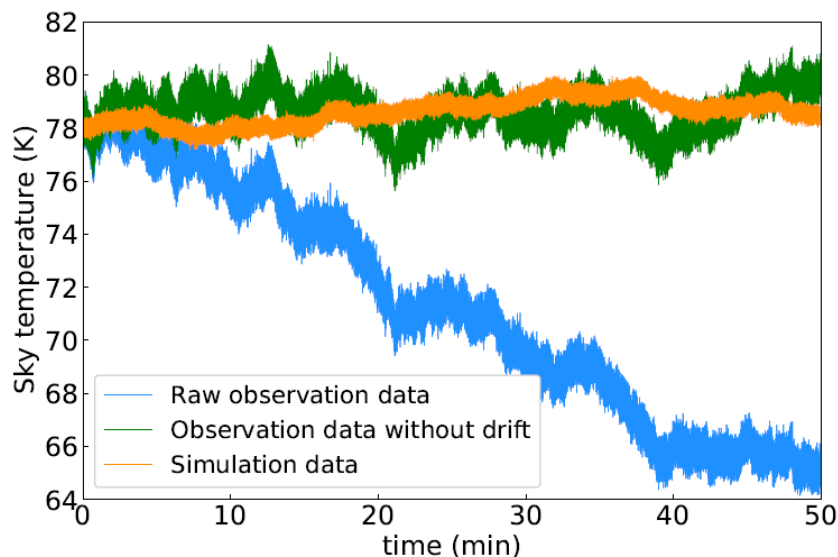


Figure 3.1: Plot of DESHIMA 1.0 observation (blue) and TiEMPO simulation (orange) data. For better comparison, the linear atmospheric drift has been removed from the observation data in the green plot. Obtained from [1].

¹See Appendix B for specifications of DESHIMA 1.0 parameters for TiEMPO

Two notable differences can be observed between the simulated and measured T_{sky} data:

Most notably, a distinct linear drift in the measurement data is visible, whereas the simulated data does not include this. This drift in sky temperature is most likely due to a shift of the precipitable water vapor during measurement, which causes the Extra Path Length to drop along with it. At the time of writing, TiEMPO is unable to simulate such a drop in precipitable water vapor. Instead of adding this drift to the input data of TiEMPO, it is far easier to remove the drift from the measurement data, which is exactly what has been done to obtain the green curve in Figure 3.1. The effects of this atmospheric drift will be important throughout the rest of this report and will turn out to be of significant importance for the choice in observation strategy in Chapter 4.4.

Additionally, when looking more closely at both the orange and green plots, a slight difference in fluctuation can be spotted: The low-frequency and large amplitude fluctuations are due to atmospheric noise, which we have seen in Chapter 2.2.1, whereas the high-frequency and small amplitude fluctuations are due to photon noise [4]. When comparing either of these fluctuations from the simulated data with the measurement, an offset of ≈ 1.6 is observed. The reason for this slight offset will be discussed more closely in the next section.

3.2. POWER SPECTRAL DENSITY

The power spectral density, or *psd* for short, is used to visualise at which frequencies the variations, i.e. noise, are strong and at which they are weak. Hence it is useful to compare the *psd* of both the measurement and simulation data, to evaluate whether TiEMPO adds the photon and atmospheric noise correctly.

The *psd* can be calculated in a variety of ways, but in this report we will stick to 2 methods: Firstly, the *psd* can be calculated directly from the T_{sky} data from either the measurement or simulation output. When the *psd* is calculated using this raw T_{sky} data, it will be denoted as psd_T . However, if the T_{sky} data is first converted into the Flux Density (F_v), it will be denoted as psd_F . Furthermore, the flat level of the *psd*, i.e. the region after which the *psd* flattens to an almost constant value, of both of these methods will be defined as S_T and S_F respectively. The significance of these flat levels will become clear in Chapters 3.2.3 and 3.3.

Note that, in this report, the *psd* spectra will be computed using the DESHIMA code for data analysis, *De:code* [16].

3.2.1. FLUX DENSITY

To determine the psd_F , the Flux Density (F_v) has to be calculated. The Flux Density is defined as the power per unit area, i.e. flux, per unit bandwidth and can be calculated via

$$F_v(T) = \frac{P_v(T)}{A_e \eta_{\text{atm}}} \quad (3.1)$$

where P_v the Power Density, A_e the Effective Area and η_{atm} the atmospheric transmission coefficient is. This transmission coefficient is the same as the one discussed in Chapter 2.2.

Using the formula for A_e , which is defined as

$$A_e = \frac{\eta_{\text{MB}} \lambda^2}{\Omega_{\text{MB}}} \quad (3.2)$$

equation 3.1 can be rewritten into

$$F_v(T) = \frac{P_v(T)\Omega_{\text{MB}}}{\eta_{\text{MB}}\lambda^2\eta_{\text{atm}}} \quad (3.3)$$

where Ω_{MB} the solid angle of main beam, η_{MB} the main beam efficiency and λ the wavelength of the observed radiation is [6][17]. The two variables concerning the main beam are defined by the telescope used. Using the fact that the ASTE telescope is used for DESHIMA measurements, the values are $\Omega_{\text{MB}} = 1.9 \cdot 10^{-8} \text{ sr}$ and $\eta_{\text{MB}} = 0.34$. Note that, typically, F_v is expressed in Jansky units ($1 \text{ Jy} = 10^{-26} \text{ Jm}^{-2}\text{s}^{-1}\text{Hz}^{-1}$).

In order to evaluate equation 3.3 and in turn to calculate the psd_F curve, the Power Density P_v has to be determined. There are two ways to do so, which will be discussed in the next section.

3.2.2. POWER DENSITY

The Power Density, denoted as P_v , can be determined via either the **Johnson-Nyquist** or **Rayleigh-Jeans** method:

When using the Johnson-Nyquist method, the Power Density is defined as

$$P_v^{JN}(T) = \frac{2hF}{e^{\frac{hF}{kT}} - 1} \quad (3.4)$$

whereas the Rayleigh-Jeans method uses the following expression:

$$P_v^{RJ}(T) = 2kT \quad (3.5)$$

In both of the expressions above, $k = 1.38064852 \times 10^{-23} \text{ m}^2\text{kg}\text{s}^{-2}\text{K}^{-1}$ is Boltzmann's constant, T is the temperature, $h = 6.62607004 \cdot 10^{-34} \text{ m}^2\text{kg}\text{s}^{-1}\text{Hz}^{-1}$ is Planck's constant and F is the frequency.

There are, however, some remarks that have to be made regarding equations 3.4 and 3.5:

1. The Rayleigh-Jeans method is an approximation of the Johnson-Nyquist method and can only be used in the limit of $hF \ll kT$ (i.e. the photon energy has to be much lower than the temperature energy of the system).
2. The Power Density P_v is also used for psd_T calculations, be it in a slightly different way: Instead of using the T parameter, the value of $\sqrt{S_T}$ is used in equations 3.4 and 3.5. For the Rayleigh-Jeans method, this does not result into significant problems, but in the Johnson-Nyquist method it will: Substituting T_{sky} with $\sqrt{S_T}$ will result in a non-dimensionless exponent in equation 3.4, thus becoming a non-physical expression. Therefore, the Johnson-Nyquist method can only be used in combination with the psd_F calculations, as defined above.
3. As TiEMPO utilises the Johnson-Nyquist method to compute the T_{sky} data, problems might arise when applying the Rayleigh-Jeans method on the simulation's output data. This is because the Johnson-Nyquist formula gives a much lower brightness temperature than the Rayleigh-Jeans temperature would. If this lower temperature is then analysed using the Rayleigh-Jeans method afterwards, a significant difference in output is observed.

Combining remarks 2 and 3, it is concluded that the Johnson-Nyquist, and thus the psd_F method should be used to correctly analyse the output data of TiEMPO. Therefore, the next section will only use the psd_F analyses of the measurement and simulation data.

3.2.3. SIMULATION VERSUS MEASUREMENT

Combining equations 3.3 and 3.4 results into the following final formula for the Flux Density, with which the psd_F curves of both the measurement and simulation data will be calculated:

$$F_v^{JN}(T_{\text{sky}}) = \frac{2\Omega_{\text{MB}}}{\eta_{\text{MB}}\lambda^2\eta_{\text{atm}}} \frac{hF}{e^{\frac{hF}{kT_{\text{sky}}}} - 1} \quad (3.6)$$

In Figure 3.2 the final plot of the psd_F of both the measurement and simulation data are plotted, together with their corresponding flat-levels S_F .

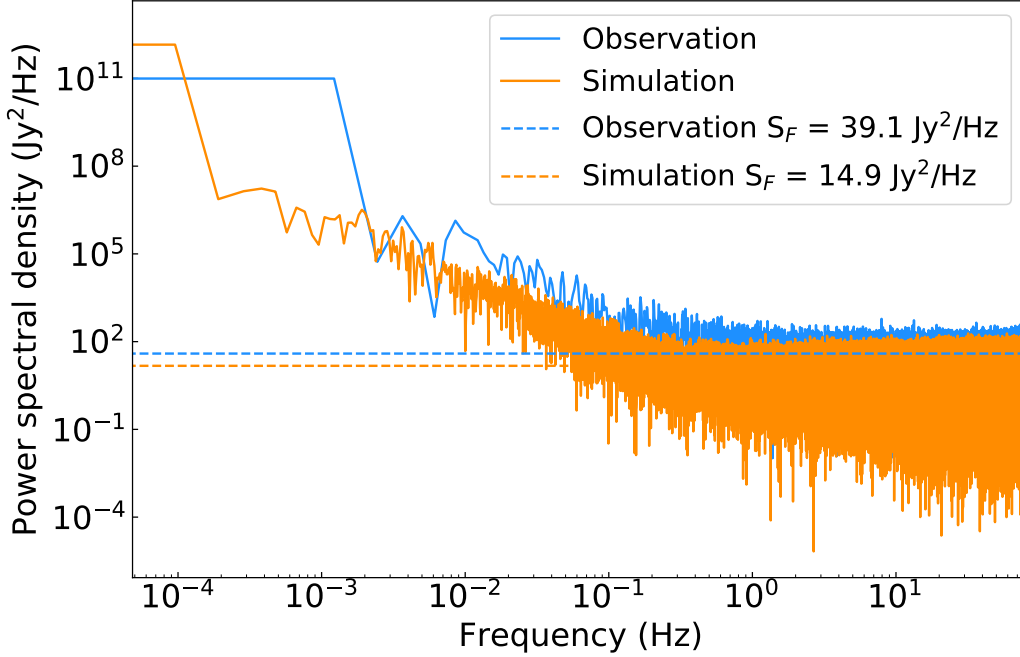


Figure 3.2: A plot of the psd_F curves of both the measurement (blue) and raw data (orange), calculated using T_{sky} data from the 350 GHz spectrometer. The dashed lines indicate the corresponding flat-levels (S_F) of both data sets.

Looking at Figure 3.2, two distinct sources of noise can be observed: For frequencies < 1 Hz, the so-called $1/f$ - noise [18], indicated by the downwards slope of the psd_F for these lower frequencies and generated by the slowly fluctuating atmospheric noise, dominates. On the other hand, the photon noise starts to dominate for frequencies > 1 Hz, as indicated by the flattening of the psd_F spectrum. The frequency that indicates the switch from $1/f$ to photon noise is called the *knee frequency* (F_{knee}), which has a value of 1 Hz in our case. The fact that both noise spectra have very similar looking shapes indicates that TiEMPO accurately simulates both the atmospheric and photon noise.

The alignment is, however, not perfect: Taking into account that both of the previously mentioned noise sources had an offset of ≈ 1.6 in Figure 3.1, it is rather interesting to see that the flat-levels of the psd_F curves in Figure 3.2 have an offset of $39.1/14.9 \approx 2.6$, bearing in mind that $\sqrt{2.6} \approx 1.6$. This correlation does not come as a surprise, as the psd_F curves are created using the T_{sky} with the same noise source offsets present. The presence of this offset in the first place is, however, unexpected.

In order to determine the origin of this unexpected S_F offset, the S_F values for all 49 spectrometers of DESHIMA 1.0 were calculated and compared of those from the TiEMPO simulation. In Figure 3.3, the results of this analysis are shown.

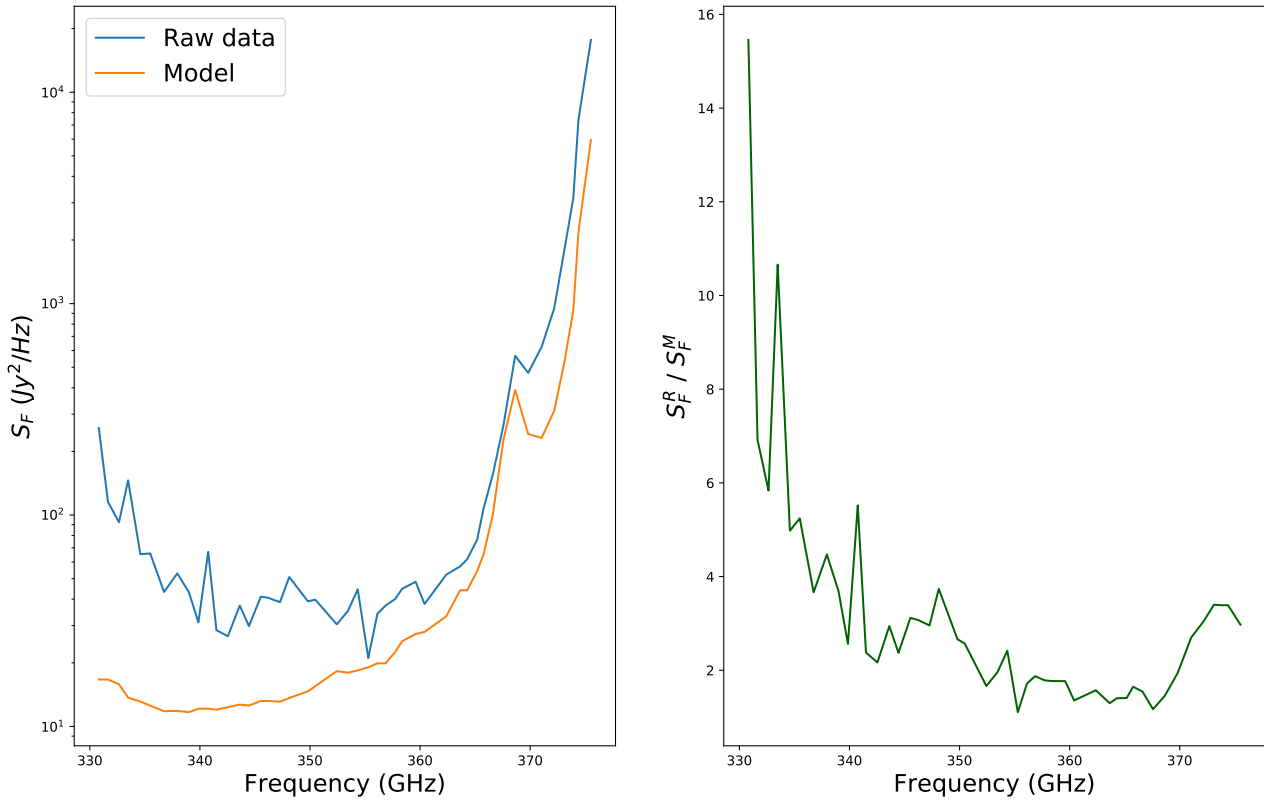


Figure 3.3: **left:** For each of the spectrometers, the S_F values for both the raw data (blue) and model (orange) are plotted. **right:** The relative offset, defined as Raw data / Model, for these S_F values is plotted.

The offset in S_F does appear to fluctuate heavily over the range of all the 49 spectrometers, and thus is not dependent on just the observation data. Kaushal Marthi, intern at SRON at the time of writing, has performed a more detailed analysis of the S_F offset, taking into account the lab-measured, channel-dependent values of the channel bandwidth, as well as adding additional instrument-related noise sources [19]. Additionally, TiEMPO utilises a single value for the optical efficiency of each of the spectrometers. This is not the case with the real measurement data, as each channel of DESHIMA 1.0 has its own optical efficiency. An illustration of this can be seen in Figure 3.4.

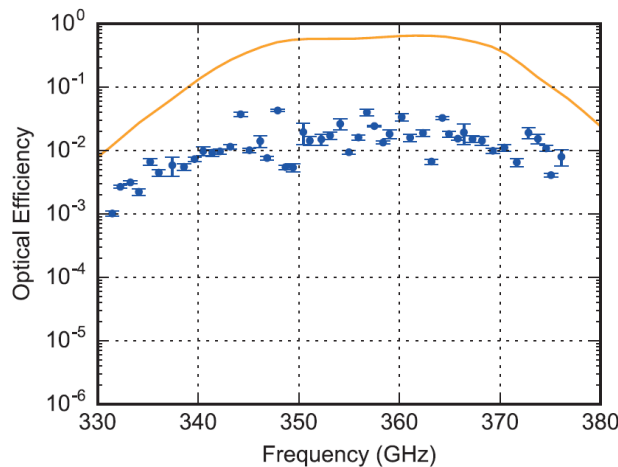


Figure 3.4: Plot of the optical efficiency of the filters (blue) versus the quasi-optical filter transmission (orange) for DESHIMA 1.0. Obtained from [20].

Combining the analysis of both Kaushal Marthi and the differences in optical efficiency suggests that the S_F offset disappears when simulating a more realistic spectrometer model.

3.3. NOISE-EQUIVALENT FLUX DENSITY

Lastly, the simulation and measurement data will be compared based on their individual Noise-Equivalent Flux Density, or *NEFD* for short. The *NEFD* of a system is an indication of the amount of flux density to be required to be equivalent to the amount of noise in the system, and is thus often used as a measurement of accuracy of astronomical observations [21].

As the Noise-Equivalent Flux Density is dependent on which type of *psd* calculation has been used before, the *NEFD* used in this report will only be based on the Johnson-Nyquist *psd_F* method. In that case, the *NEFD* is defined as

$$NEFD = \sqrt{\frac{S_F}{2}} \quad (3.7)$$

where S_F is the flat level of the *psd_F* curves.

Using this definition for the Noise-Equivalent Flux Density, the *NEFD* is calculated and plotted in Figure 3.5, using both a Lorentzian [22] smoothed and unsmoothed η_{atm} . In the Figure, the *NEFD* data of DESHIMA 1.0 measurements of the VV114 and IRC 10216 galaxies are added too, for comparison. In addition, the *NEFD* calculated using the static *Deshima-Sensitivity* model is added [23].

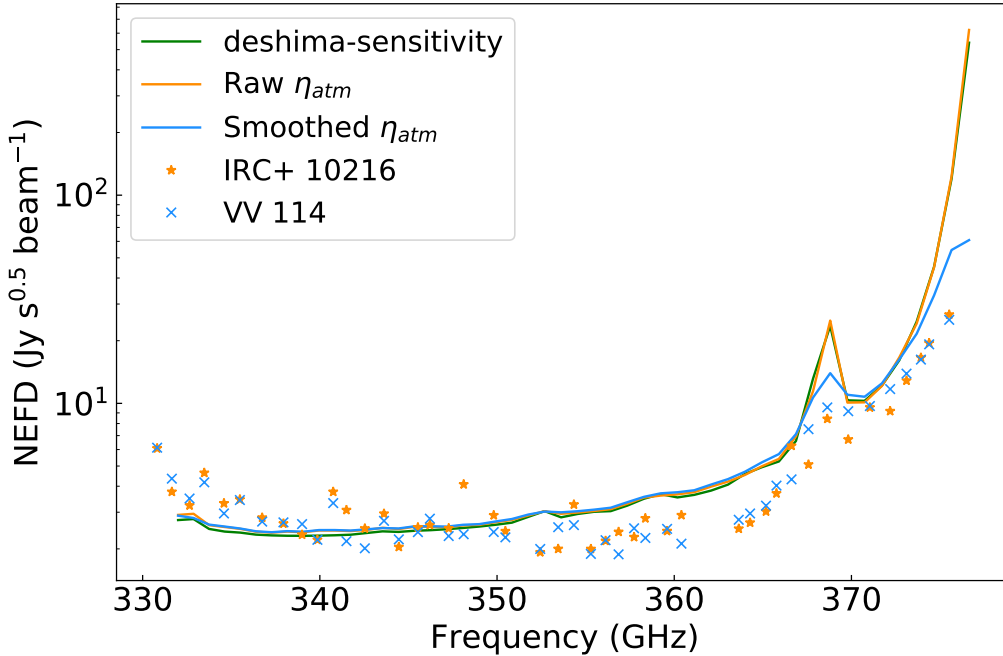


Figure 3.5: *NEFD* plot of the output data of TiEMPO using a smoothed (blue) and raw (orange) atmospheric transmission coefficient, η_{atm} . In addition, the *NEFD* data of the VV 114 (blue marker) and IRC 10216 (Orange marker) galaxies, measured with the DESHIMA 1.0 spectrometer, are added. Lastly, a simulation using the static *Deshima-Sensitivity* model is added.

The TiEMPO curves are made with both a raw and smoothed η_{atm} , because of several reasons: Firstly, the static *Deshima-Sensitivity* model utilises a raw atmospheric η_{atm} in its calculations, so in order to compare TiEMPO accurately with this model, a raw η_{atm} has to be used. On the other hand, the real measurement data are used with a continuous atmospheric transmission, making a smoothed η_{atm} preferable for comparison.

As illustrated in Figure 3.5, the TiEMPO simulation which uses a raw η_{atm} (orange line) shows great resemblance with the static *Deshima-Sensitivity* model (green line). However, both curves have distinct offsets with comparison with the real measurement data of the galaxies VV114 and IRC 10216 (blue and orange markers). The TiEMPO simulation which uses a smoothed η_{atm} (blue line), lies a lot closer to these real data points, especially for frequencies of above ≈ 368 GHz. The reason for this is that, for frequencies of above ≈ 368 GHz, the atmospheric transmission coefficient changes rapidly, as seen in Figure 2.2. For regions with rapidly changing atmospheric transmission, the smoothing of η_{atm} creates a better representation of the continuous atmospheric window.

The reason why even the TiEMPO simulation that uses a smoothed η_{atm} is not perfectly in agreement with the observation data has multiple possible reasons: Firstly, the measurements of DESHIMA 1.0 used to determine the galaxies' *NEFD* data points took multiple days, with significant atmospheric changes during the observations. TiEMPO, however, simulates the atmospheric data for the much shorter amount of time of ≈ 8 hours, with relatively constant atmospheric conditions. Additionally, the difference in optical efficiency between the simulated and measurement optical efficiencies, as discussed in the previous section and illustrated in Figure 3.4, imposes an offset between the *NEFD* plots.

Altogether, TiEMPO shows great potential regarding simulation of Earth's atmosphere, and can correctly interpret it into the noise this adds to the observation data. Even though improving TiEMPO with a more detailed and realistic instrumental simulation will result into an even more accurate simulation, the atmospheric model used within TiEMPO already simulates real-world conditions with a reasonable accuracy.

4

OBSERVATION SIMULATIONS

With the accuracy of TiEMPO analysed and verified, it is time to start applying the simulation on galaxy observations. In order to do so, two observation strategies regarding different chopping techniques will be evaluated: The Dual and ABBA chopping techniques.¹ Before analysing the effect of these observation methods, the principal behind both of them will have to be explained first: sky chopping.

4.1. SKY CHOPPING

Chopping is used during ground-based observations as an effective way of filtering out any atmospheric noise. Even though there are several ways to do so, all chopping techniques rely on the same principal: by observing towards the galaxy in question, the telescope observes both the galactic and atmospheric data. This position is the so-called *ON* position, as the telescope beam is "on" the galaxy. After staying for some time on the *ON* position, the telescope beam is chopped away from the *ON* position, and starts measuring the so-called *OFF* position, i.e. a position where the telescope beam does not include the galactic data. The beam separation, i.e. the angle between the beams observing either *ON* or *OFF*, should be large enough such that there is no overlap in the far-field, whilst at the same time having as much overlap as possible in the near-field. A visualisation of the far- and near-field of sky chopping is given in Figure 4.1.

Because the *ON* and *OFF* beams have no overlap in the far-field, but have good overlap in the near-field, the difference between the two beams will contain significantly less atmospheric noise, while preserving the galactic data. In order to visualise the effectiveness of beam separation as an atmospheric noise filter, Figure 4.2 illustrates the effect of the *ON* and *OFF* beams in the near field of an ARIS simulation.

Even though the beams are completely separated in the far-field, there is a significant amount of overlap in the near-field. The effectiveness of eliminating the atmospheric noise is strongly dependent on the similarity between the area of the atmosphere observed by the two telescope beams. After all, if the *OFF* beam contains a completely different part of the atmosphere, the atmospheric noise cannot be filtered out by looking at the difference between the two beams.

In order to allow for simulations of the effect of different chopping techniques, TiEMPO simulates 5 positions of atmospheric observation at the same time: 4 *OFF* positions surrounding 1 *ON* position in the centre, as illustrated in Figure 4.3. The 4 *OFF* points used in TiEMPO will, in the remaining part of this chapter, be denoted as *L*, *R*, *T* and *B*, representing the left, right, top and bottom *OFF* points, respectively. The centre / *ON* chopping point will be denoted as *C*.

¹Equivalent to Figure 3.1, the measurement and simulation data used for these observation simulations will contain 50 minutes of data each

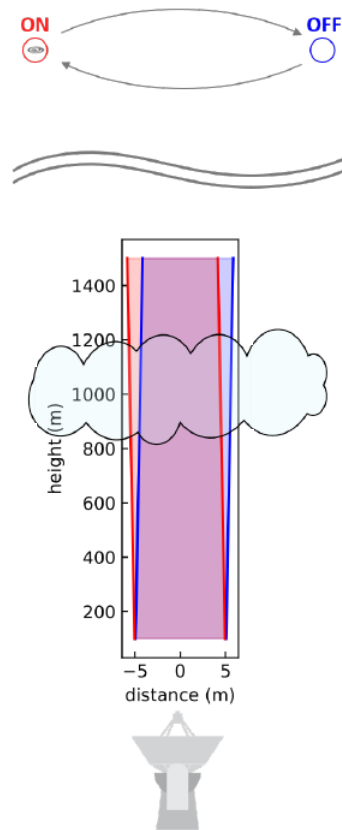


Figure 4.1: A visualisation of Sky Chopping, obtained from [1]. In the far-field, the beams of the ON and OFF positions are completely separated, whereas in the near-field, these beams do overlap.

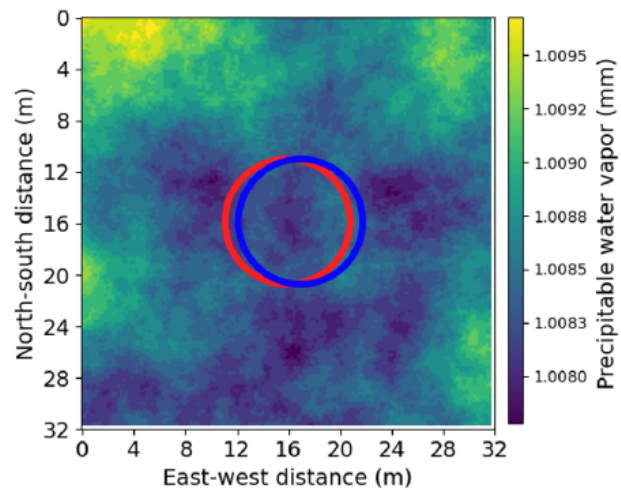


Figure 4.2: Visualisation of the ON (red) and OFF (blue) telescope beams in the near field. The beams have been placed upon a section of ARIS data, illustrating the minimal effect of the beam separation in the near field. Obtained from [1].

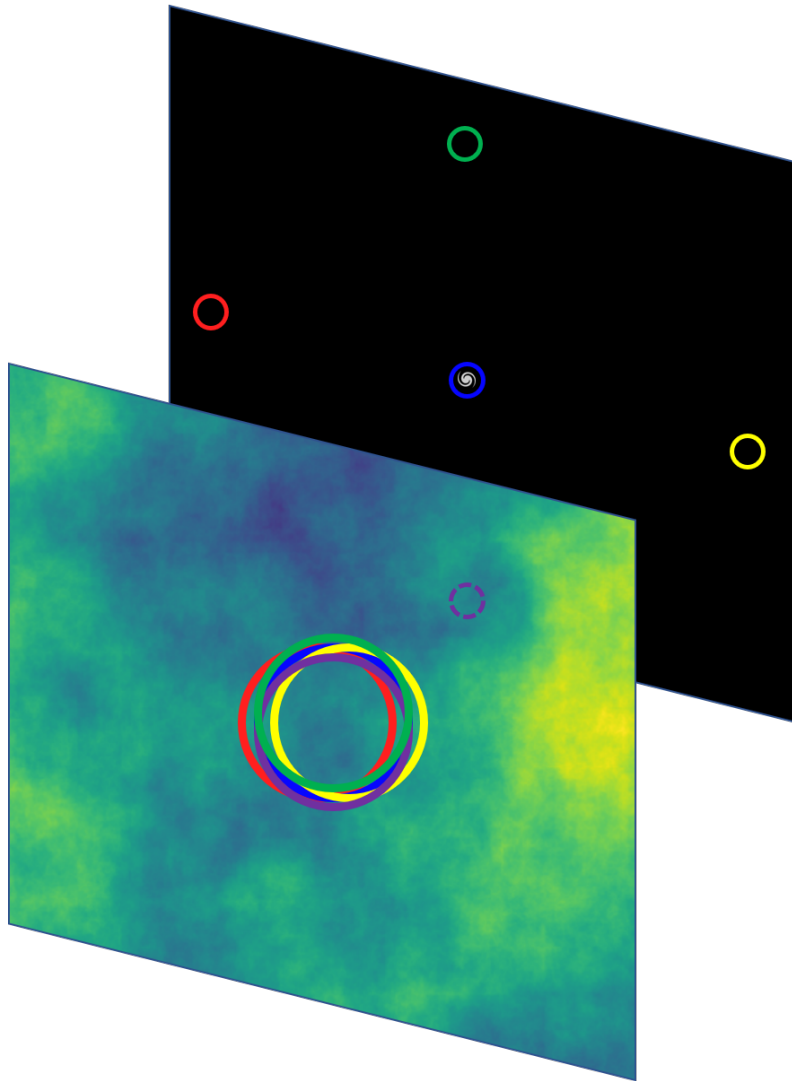


Figure 4.3: Visualisation of the 5 chopping positions used by TiEMPO in both the near- and far-field of the telescope. The galaxy is positioned in the centre, i.e. the ON position. The four points surrounding the centre position are the so-called OFF positions. Obtained from [1].

4.2. DUAL CHOPPING

Dual chopping is more straightforward than ABBA chopping, as it simply involves alternating between 1 ON and 1 OFF point, hence the name of the chopping method. After the chopping points have been observed for a certain amount of time, the difference between the ON and OFF points is taken.

4.2.1. EFFECTS OF ATMOSPHERIC CHANGES

Before using the output data of TiEMPO as a baseline for observation strategy recommendations, the usability of the data has to be analysed. At first, this will be done by performing a dual chopping simulation on both real measurement and simulation data and comparing the two chopping simulations. As the measurement data used for this is a so-called 'still-sky' measurement, i.e. a measurement involving no telescope movement and without any galaxy signals, the dual chopping simulation will be performed with just one chopping position. As the galaxy signal is not included in the 'still-sky' data, all five chopping positions are, in principle, OFF points. Even though using a single chopping position greatly improves the similarity of observation conditions between measurement and simulation, any possible effects of spatial differences of the atmosphere are neglected. However, as no galaxy signal is present, it is a perfect test to analyse whether the dual chopping technique can effectively filter out the atmospheric noise. In Figure 4.4 the results of this 'still-sky' OFF-OFF chopping is plotted for a variety of chopping times, i.e. the time the telescope stays on one chopping position. As the measurement data (top plot in Figure 4.4) contains an atmospheric linear drift, as illustrated in Figure 3.1, a similar drift has been added to the data acquired from TiEMPO (bottom plot in Figure 4.4).

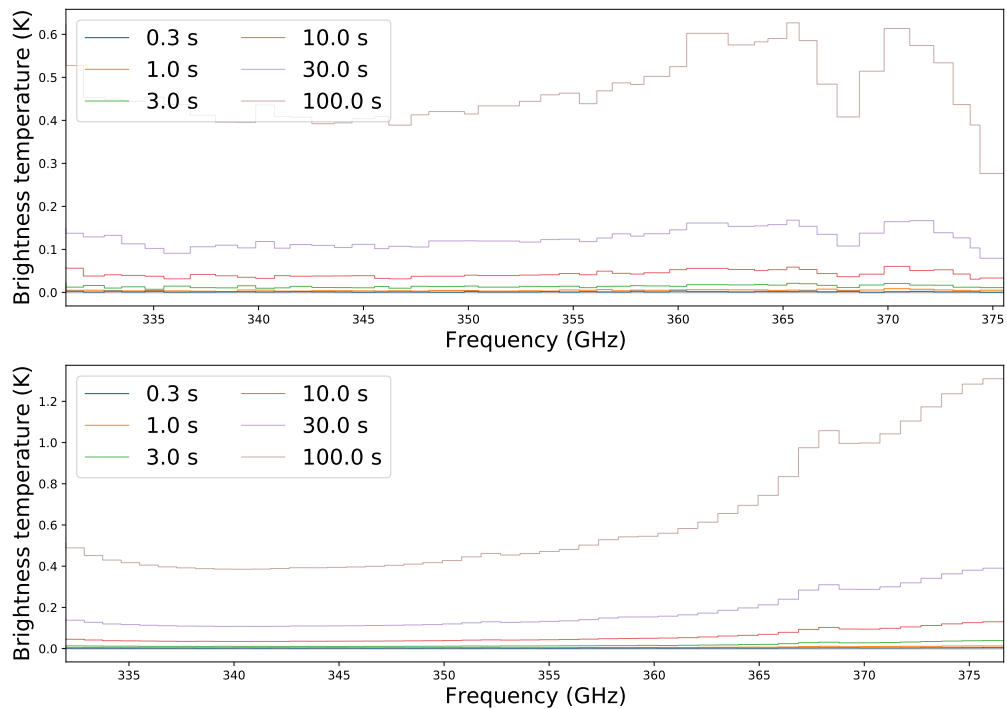


Figure 4.4: **Top:** Plot of the dual chopping technique, applied to the measurement data of the 'still-sky' measurement of DESHIMA 1.0 for different chopping times. **Bottom:** Plot of the same dual chopping method but applied to the output data of TiEMPO with an atmospheric drift added to it. Both plots are made using an OFF-OFF dual chopping method. In addition, neither of the data sets used contains a galaxy.

At first glance, the two images plotted in Figure 4.4 show little similarity. However, for both the TiEMPO and measurement data, there is an offset of the resulting OFF-OFF spectrum which scales with the chopping time. Even though it might seem contradictory to see a non-zero result when subtracting data from the same spatial point, this is not surprising: during longer chopping times, the atmosphere is given more time to change, which in turn decreases the efficiency of the noise filtering. This effect is enhanced by the linear atmospheric drift present in both the measurement and simulated data, as it causes the atmospheric conditions of the measurement data to change more rapidly over time. Therefore, the dual chopping technique is most efficient for lower chopping times, where this offset is still relatively small.

Despite the fact that the offsets of the two plots are fairly similar and can be explained using the atmospheric drift, the difference in shape of the two plots in Figure 4.4 is less straightforward: While the measurement data (top) shows a wave pattern, the simulation data (bottom) shows an ever increasing peak after ≈ 360 GHz. After closer inspection, the difference in shape of the two plots was found to be originating from the way the atmospheric drift was added to the simulation data: The drift added to the TiEMPO data was equal for all spectrometer channels, whereas the amount of drift on each of the channels should be added accordingly. In addition, not only the atmospheric noise, but also the photon noise was altered during the addition of the atmospheric drift, which is not physically correct. For a few future plots in this paper that contain the same artificially added atmospheric drift, the effect of this faulty implementation of the atmospheric drift have been analysed and plotted in Appendix C. This analysis showed that the effects of this incorrectly implemented drift are minor and will not influence the conclusions that will be drawn from the data significantly. For a more accurate and correct atmospheric addition, the atmospheric drift has to be added as a drift in pvv before being processed by TiEMPO.

4.3. ABBA CHOPPING

In order to filter out the atmospheric noise more efficiently, the ABBA chopping method can be applied. This commonly used astronomical observation method utilises three chopping positions, 1 ON and 2 OFF. These three positions are grouped in two ON-OFF pairs, called *nods*, between which the telescope performs an alternating dual chopping method. A good illustration of this is given in Figure 4.5.

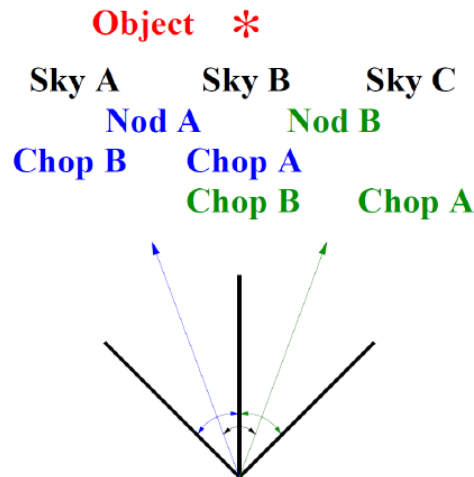


Figure 4.5: Illustration of an ABBA chopping observation. The three sky positions, denoted with Sky A, B and C are grouped into two pairs of two. These pairs are denoted as Nods A and B, between which the telescope will alternate over a specified nodding interval. At each of the nodding positions, the telescope will perform a dual chopping method, with a distinct chopping interval. Obtained from [24]

The telescope will perform a dual chopping method between the chopping positions Sky A and B while being located in nodding position A, before switching to nodding position B and performing a similar chopping

4.3.1. MEASUREMENT VS TIEMPO

Before applying the ABBA chopping technique, its ability to remove the atmospheric linear drift has to be verified for both data acquired from DESHIMA 1.0 measurements and from TiEMPO. This is done by performing a 'stationary' chopping technique. This stationary technique uses the same algorithm as the one illustrated in Figure 4.6, but all three of the used data sets are from a singular sky chopping position. This means that the filtration of sky data is only influenced by the temporal differences between the used data parts. In Figure 4.7, the data from position *C* is used, similar to the procedure used in Chapter 4.2. Again, the 'still-sky' measurement data will be used, which does not contain any galactic data.

In addition, a single chopping frequency of 10 Hz is used, while the nodding frequency is varied over a range of different values. The choice of this specific chopping frequency is based on the requirements of the DESHIMA 2.0 spectrometer: As seen in Chapter 3.2.3, the F_{knee} for atmospheric noise is ≈ 1 Hz, which would indicate that the minimum chopping frequency of 1 Hz is needed to filter out the noise. However, the DESHIMA 2.0 spectrometer is also influenced by $1/f$ KID noise, which has a F_{knee} that is typically a bit higher than 1 Hz. As the chopping frequency has to be higher than either of the two F_{knee} values, a chopping frequency of 10 Hz has been chosen for applications of the ABBA chopping simulation.

The results of simulating the stationary ABBA chopping method with the measurement data is shown in Figure 4.7.

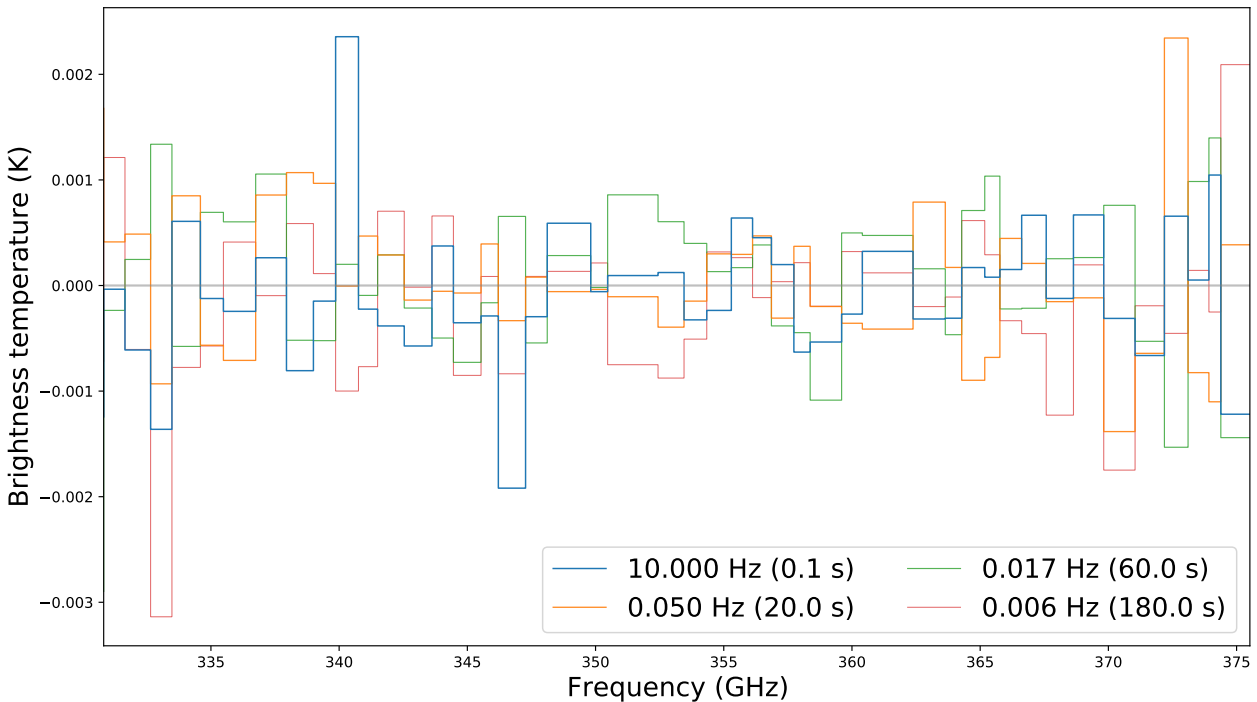


Figure 4.7: Stationary ABBA chopping method applied to the measurement data of DESHIMA 1.0. The plots are created by varying the nodding frequency, while keeping the chopping frequency on a single value of 10 Hz. As the measurement data is 'still-sky', it does not contain any galaxy signal.

An interesting phenomenon can be observed in Figure 4.7: All curves show rapid changing fluctuations around zero, which indicates that the effects of the linear drift have been removed.

To check if this is the case for simulated data as well, a plot is made using the same stationary ABBA method, but this time applied to output data of a TiEMPO simulation without a galaxy. In addition, the linear drift is added to the TiEMPO data, to better simulate the actual measurement data.² If the ABBA method works as anticipated, the results of the TiEMPO data, plotted in Figure 4.8, will look very similar to those of the measurement data, plotted in Figure 4.7.

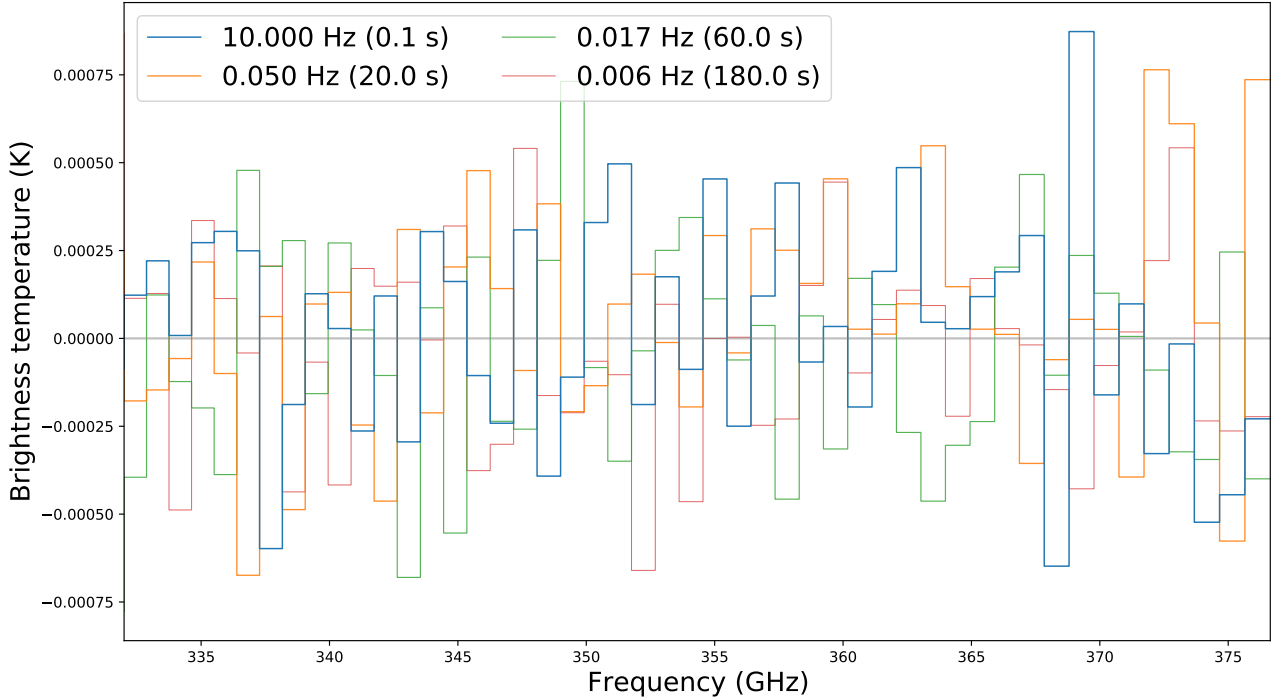


Figure 4.8: Stationary ABBA chopping method applied to output data of TiEMPO. The nodding frequency is again varied, while the chopping frequency is set on a single value of 10 Hz. Just like before, no galaxy is added to the atmospheric data.

Just as expected, the ABBA simulation shows a very similar set of plots for both the data created by TiEMPO (Figure 4.8) and DESHIMA 1.0 measurement data (Figure 4.7). It is therefore safe to assume that the applied ABBA chopping is able to remove the linear atmospheric drift for both measurement data and data acquired from TiEMPO equally well.

4.4. CHOICE OF CHOPPING METHOD

Choosing the correct chopping method is crucial before starting an observation campaign, as it can influence the observation length needed and quality achieved drastically. In addition, not all telescopes are equipped with the instruments needed to do fast nodding and chopping movements, limiting the maximum speed at which an observation can be executed. Therefore, more complex chopping strategies such as ABBA chopping should be avoided if they do not result into significant improvements on the output data.

In this section, measurement data of DESHIMA 1.0 and simulation data of TiEMPO will be used to determine whether the ABBA chopping technique is indeed a necessity for high quality galaxy observations of DESHIMA 1.0 and 2.0, or whether the simpler dual chopping method yields similar results.

²See Chapter 4.2.1 and Appendix C for more information about this artificial drift

4.4.1. DESHIMA 1.0

In order to determine which chopping technique to use for DESHIMA 1.0 observation, the effects of each of the techniques have to be compared under similar measurement circumstances. After all, the ABBA simulations in Chapter 4.3.1 were performed with a chopping frequency of 10 Hz. On the other hand, the dual chopping simulation of Chapter 4.2.1 showed that for short chopping times, and thus high chopping frequencies, the dual chopping simulation was least affected by the effects of both the linear atmospheric drift and the spatial differences between chopping points.

Hence, in order to determine whether the ABBA chopping technique is necessary for DESHIMA 1.0 observations, an ABBA chopping simulation with a nodding time of 60 s is plotted together with a 10 Hz dual chopping simulation in Figure 4.9. Both plots use again the DESHIMA 1.0 measurement data, which is stationary and does not contain a galaxy signal.

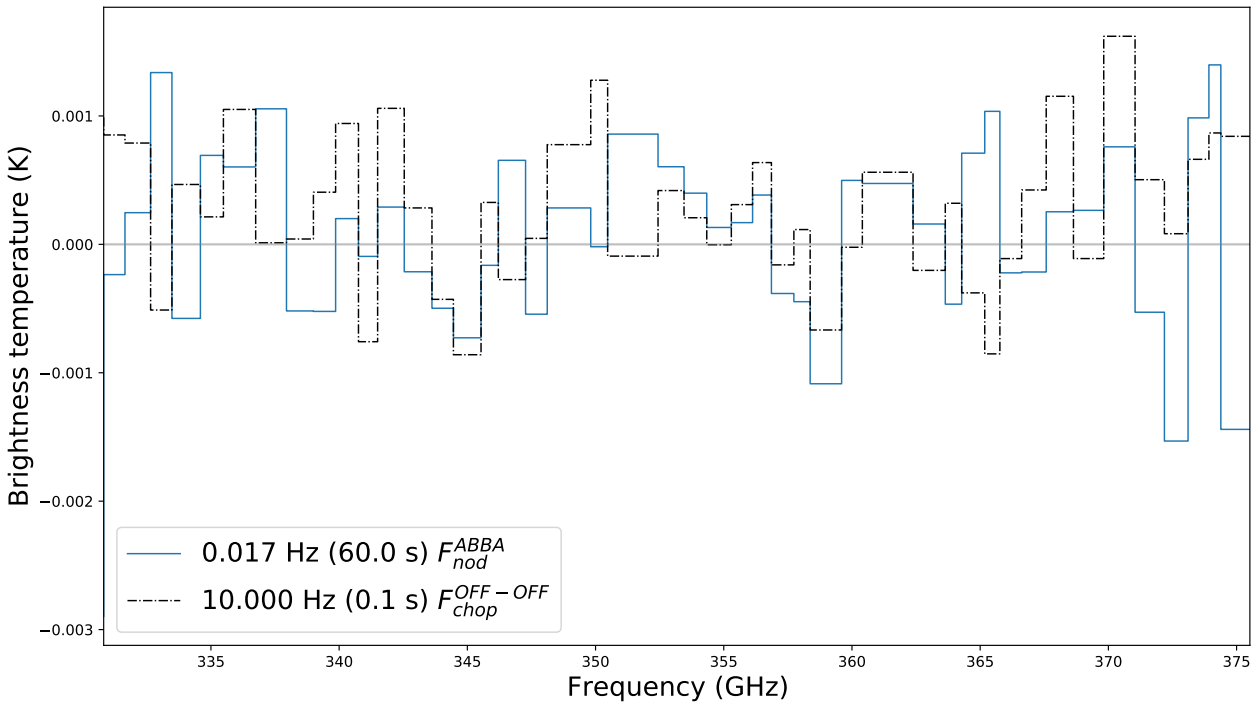


Figure 4.9: ABBA simulation plots for a nodding time of 60 s (blue line), together with a dual chopping simulation with a chopping frequency of 10 Hz (black dash-dotted line). The plots are created using 'still-sky' DESHIMA 1.0 observation data, which does not include galaxy signal.

When looking at Figure 4.9, no distinct differences between the two chopping simulations are visible. After all, both the ABBA and dual chopping simulation lead the expected plot of fluctuations around zero. This indicates that the implementation of an ABBA chopping technique with DESHIMA 1.0 measurements is not recommendable with the applied measurement conditions and observation time of 50 minutes, as it does not result into significant improvements of the filtration of the atmospheric noise. We do have to bear in mind that, if we were to perform a similar analysis with longer observation times, we might observe a different outcome.

4.4.2. DESHIMA 2.0

As the DESHIMA 1.0 TiEMPO and chopping simulations could be compared with the real measurement data of DESHIMA 1.0, it was the perfect way to test the validity of both of these simulations. However, for DESHIMA 2.0, this is not the case, as the DESHIMA 2.0 chip has yet to start its first observation campaign. Therefore, the fact that the DESHIMA 1.0 simulations earlier in this paper have proven the accuracy of both the TiEMPO and chopping simulations indicates that these simulations can be used to simulate DESHIMA 2.0 observations as well. In order to choose between which chopping technique to use for galaxy observations (see next section), this section will only use data that contains no galaxy signal and that has been created using TiEMPO with DESHIMA 2.0 parameters.³

By adding a linear drift to the output data of TiEMPO, a simulation similar to the one in Figure 4.9 can be performed to determine the effectiveness of ABBA chopping for DESHIMA 2.0 observations.⁴ The output of this simulation is plotted in Figure 4.10.

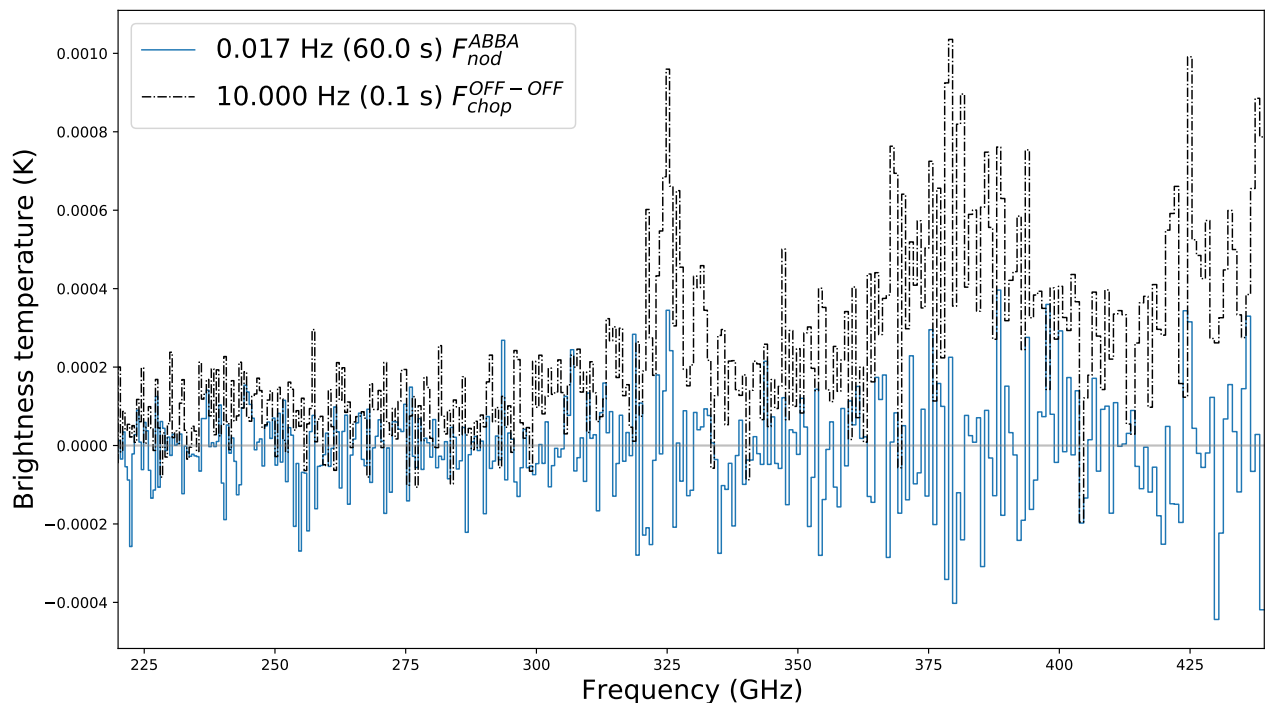


Figure 4.10: Plot of an ABBA chopping simulation (blue) and a dual chopping simulation (black) of DESHIMA 2.0 observation data simulated by TiEMPO. The offset of the dual chopping simulation indicates that it is unable to remove all effects of the linear drift present in the data, resulting in a distinct improvement of the output of the ABBA chopping technique.

As opposed to DESHIMA 1.0 observations, Figure 4.10 illustrates that the ABBA chopping technique does add an improvement of the observation spectra of DESHIMA 2.0 observations: Whereas the ABBA simulation (solid blue) nicely fluctuates around zero, shows the dual chopping simulation (dashed black) an offset from the zero line. This indicates that the linear drift cannot be compensated anymore with the chopping frequency of 10 Hz for the dual chopping method. This indicates that the ABBA technique is indeed needed for high-quality DESHIMA 2.0 observations.

³See Appendix B for specifications of DESHIMA 2.0 parameters for TiEMPO

⁴Again, See Chapter 4.2.1 and Appendix C for more information about this artificial drift

Additionally, the DESHIMA 2.0 observation simulation does not have to be performed with only a stationary ABBA strategy. Hence, a simulation of a dynamical⁵ ABBA chopping strategy is performed as well: Using data from TiEMPO's *L*, *C* and *R* chopping points, Figure 4.11 illustrates the outcome of this dynamical observation simulation.

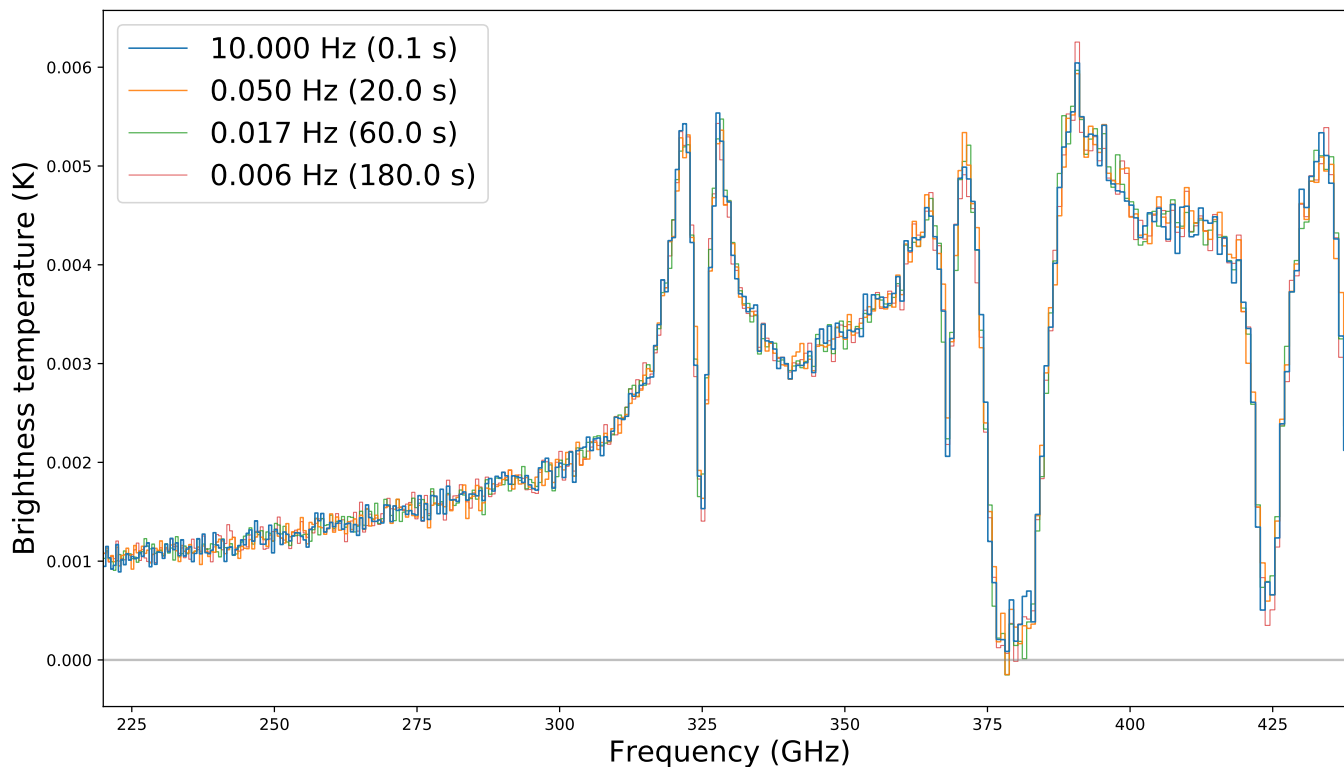


Figure 4.11: A plot of a dynamical ABBA chopping strategy, which utilises the *L*, *C* and *R* chopping points from TiEMPO. Once again, the chopping frequency is set to 10 Hz, while the nodding frequency is altered. The non-zero offset of the plot, as opposed to Figure 4.10, shows that ABBA is unable to remove the offset created by the spatial differences between observation points.

From Figure 4.11, we can draw the conclusion that, although very effective against linear atmospheric drift, ABBA is unable to remove the offset created by the spatial differences between observation points. This is illustrated by the fact that the plots in Figure 4.11 all have an offset, whereas no galaxy is present in the simulated data.

⁵Similar to the chopping sequence illustrated in Figure 4.6

4.5. DESHIMA 2.0 GALAXY OBSERVATION SIMULATION

Now that the necessity for ABBA chopping for DESHIMA 2.0 observations is demonstrated, an actual galaxy observation can be simulated. In Figure 4.12, a dynamical simulation similar to the one in Figure 4.11 is plotted. However, this time the data acquired from TiEMPO does contain a galaxy on its centre chopping point.⁶

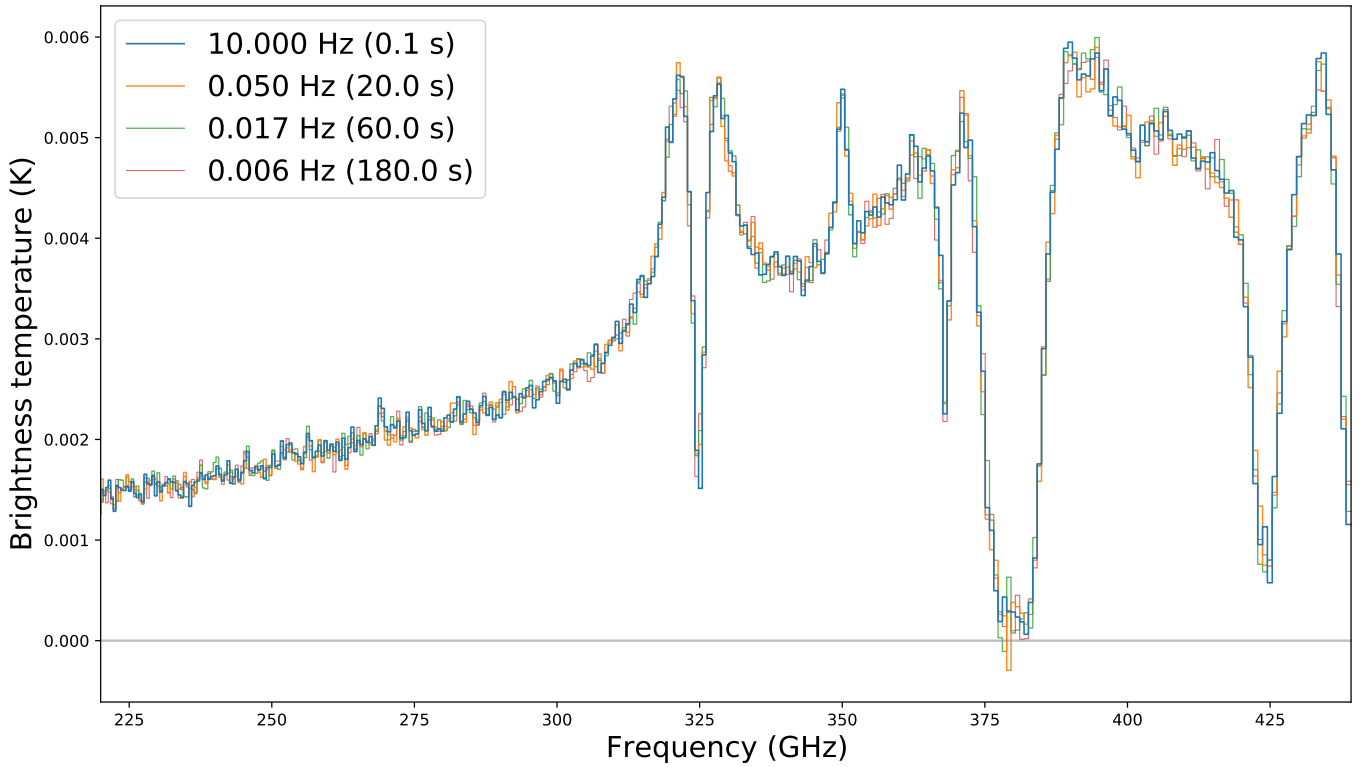


Figure 4.12: A plot of the same dynamical ABBA chopping strategy as in Figure 4.11, but this time the TiEMPO data has a galaxy positioned on its ON chopping point. Two distinct peaks can be spotted at around 270 and 350 GHz, indicating emission line observations of the galaxy.

Comparing Figures 4.11 and 4.12 shows us that the galactic data has had some major influence on the output of the dynamic ABBA simulation: Especially around the frequency values of 270 and 350 GHz, some distinct peaks can be spotted in Figure 4.12, whereas these are not visible in Figure 4.11. To better illustrate this, the difference between the spectra in with and without a galaxy signal is taken and plotted in Figure 4.13.

In addition, the spectrum we expect to see based on the input values of TiEMPO is plotted in Figure 4.13 as well. This expected spectrum is acquired by calculating the redshifted spectrum of the galaxy before any noise is added to it, after which the effects of atmospheric attenuation are added to it.⁷ Furthermore, the spectrum is smoothed with a Lorentzian filter with a FWHM, i.e. Full width at half maximum, representative of the filter bandwidth.

⁶See Appendix B for used TiEMPO Parameters and galaxy variables

⁷as illustrated in Figure 2.2

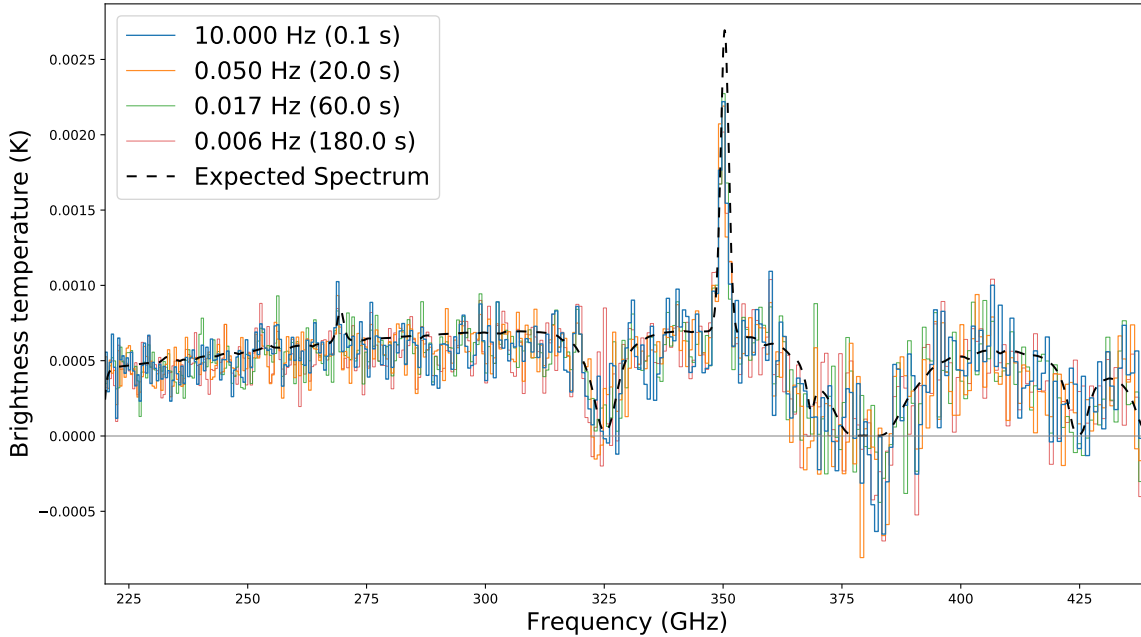


Figure 4.13: A plot showing the subtracting of the two spectra plotted in Figures 4.11 and 4.12. This subtraction shows the peak at 350 GHz even more clearly, and even shows that the continuum emission has been made visible. The black dashed line is the spectrum we expect to see based on the input values of TiEMPO and Earth’s atmosphere’s transmission spectrum.

When looking at the spectra obtained with ABBA and the expected spectrum in Figure 4.13, we can see great resemblance between them in both shape and offset. This indicates that the simulations we performed to remove the noise sources have been successful and accurate, effectively working as a last check for the applied simulations.⁸ There are, however, two small remarks to be made regarding the similarities between the spectra: First and foremost, the value of the peak at 350 GHz has a difference of $\approx 30\%$ between the expected and acquired spectra. This is most likely due to an offset between the filter peak and the astronomical line peak. In addition, the expected spectrum seems to drop at ≈ 220 GHz, which is due to the used convolution algorithm.

When looking at Figure 4.13, we can clearly see that the continuum emission of the galaxy has been made visible. This is illustrated by the fact that the entire spectrum has a positive offset, even after subtracting the non-galactic observation spectra with identical atmospheric conditions. The fact that the continuum spectrum is bumpy, i.e. dropping to zero for some frequencies, is due to the fact that the spectra in Figure 4.13 have not been corrected for atmospheric absorption. This is also the reason why the atmospheric absorption has been added to the expected spectrum, to make comparing them more straightforward.

Upon closer inspection, we find that the peaks at the frequency values of 270 and 350 GHz in the spectra of Figure 4.13 seem to originate from the redshifted [NII] and [CII] emission lines of the galaxy, respectively. Using the rest frequencies corresponding to both of these emission lines, which have values of 1461 and 1901 GHz respectively [8], the redshift of the observed galaxy can be calculated using equation 2.1. These calculations result into redshifts of $z = 4.41$ and $z = 4.43$, which correspond very well with TiEMPO’s input value of 4.43. This shows that, with the ABBA chopping technique, the redshift of a galaxy simulated with TiEMPO can be obtained with fairly high precision.

⁸Bear in mind that the type of analysis performed in Figure 4.13 is not achievable during real measurement data: After all, it is not possible to have the exact same atmospheric conditions on all three chopping positions with and without galactic data. Nevertheless, this type of spectra is what ultimately should be made visible using advanced signal processing methods, thus making it into a nice comparison for when real measurement data will become available.

5

CONCLUSIONS AND FUTURE WORK

5.1. CONCLUSIONS

In this report, we have looked at the output of the TiEMPO model and have succeeded in verifying its accuracy. In addition, we have looked at the first simulations using the output data of TiEMPO, which led to new insights regarding ground based DESHIMA observations.

To do so, we have first used TiEMPO with parameters similar to those of real measurement data acquired with the DESHIMA 1.0 spectrometer. By comparing the raw output of both the simulated and measurement data at an observing frequency of 350 GHz, a distinct linear drift was visible in the measurement data, most likely caused by a shift of the weather conditions during measurement. In addition, the magnitude of both the small and large amplitude fluctuations showed an offset of ≈ 1.6 between the measured and simulated data.

By computing and comparing the *power spectral density* (*psd*) of the measured and simulated data, the ability of TiEMPO to simulate the atmospheric and photon noise was analysed. This analysis showed the expected $1/f$ -noise region for low and the photon noise for higher frequencies, with a knee frequency of around 1 Hz. Nevertheless, an offset of ≈ 2.7 of the 350 GHz flat level *psd* is observed between the two data sets. Bearing in mind that $\sqrt{2.7} \approx 1.6$, this offset appeared to be related to the atmospheric offset observed during the previous analysis. Following the findings of Kaushal Marthi, it can be concluded that a simulation of a more realistic spectrometer model and the adjustment of the mean fluctuation of the atmosphere will result into a disappearance of these atmospheric offsets.

Lastly, the *Noise-Equivalent Flux Density* (*NEFD*) of both the measured and simulated data were calculated and compared, as well as the output of the static *Deshima-sensitivity* model. For the simulated data, both a Lorentzian smoothed and raw atmospheric transmission coefficient (η_{atm}) were used for the comparison. The raw η_{atm} data showed great resemblance with the static Deshima-sensitivity model, whereas those with a smoothed η_{atm} lied closer to the measurement data. The still present offset between simulated and measurement data is most probably due to changes in measurement conditions and the frequency-dependency of the optical efficiency of each observation channel. The results indicate that the atmospheric model used within TiEMPO is able to simulate real-world atmospheric conditions with a reasonable accuracy.

After the atmospheric model used within TiEMPO had been verified, simulations of real-life observations were performed. To do so, the Dual and ABBA chopping techniques were introduced and simulated for a non-galaxy containing measurement and TiEMPO data for DESHIMA 1.0 and 2.0. These simulations showed that the ABBA chopping technique has the potential to improve the quality of the observed spectrum for DESHIMA 2.0 measurements, but is unable to completely remove the atmospheric noise observed during measurements: More advanced signal processing techniques will have to be developed to do so.

Following the conclusions drawn from these simulations, a galaxy observation of DESHIMA 2.0 was simulated using galaxy containing TiEMPO data. In the observation spectrum, distinct peaks originating from the redshifted [NII] and [CII] emission lines were observed at frequencies of 270 and 350 GHz, which gave rise to redshifts of $z = 4.41$ and $z = 4.43$. These values found for the redshift correspond very well with TiEMPO's input value of 4.43, illustrating that TiEMPO can be used for galaxy observation simulations.

5.2. FUTURE WORK

Resulting from this report and its findings, further research regarding the precision of TiEMPO model as input parameters have to be performed. In addition, the effects of adding more realistic instrument specifications to the TiEMPO software, such as frequency-dependent optical efficiencies of the observation channels, have to be studied more closely.

To compare the measurement and simulation data of DESHIMA 1.0 more closely and to analyse the effects of the Dual and ABBA chopping techniques adequately, an artificial atmospheric drift has been added to the output data of TiEMPO. This addition has, however, been performed in a manner which is imperfect: Instead of calculating the amount of drift added to each spectrometer channel according to a common pvv drift, all channels had the same amount of drift. In addition, not only the atmospheric noise, but also the photon noise was altered during the addition of the atmospheric drift, which is not physically correct. These errors regarding the atmospheric drift addition resulted in inaccuracies regarding the dual chopping technique. Despite these inaccuracies in the addition of the atmospheric drift, the ABBA chopping technique has minimised the consequences this would have had to our conclusions regarding galaxy observations. Nevertheless, a more accurate and correct atmospheric addition has to be performed in future studies, which means incorporating the atmospheric drift as a drift in pvv in the ARIS simulation software, instead of adding this drift after applying TiEMPO.

Despite the fact that the ABBA chopping technique is capable of removing the previously mentioned linear atmospheric drift present in its input data, it is incapable of completely removing the spatial differences between observation points. In order to increase the quality of observation, the offsets resulting from these differences will have to be corrected for using advanced signal processing methods. Additionally, the dependency of these spatial offsets can be plotted against the amount of beam splitting, which will reveal to which degree precise beam splitting can help to reduce the resulting offset.

Furthermore, the spectra found with the help of the galaxy observation simulation should be reproducible using these same advanced and more realistic signal processing methods. In addition, the quality of galaxy data filtration will have to be improved for measurements involving galaxies that are much fainter than discussed in this report.

APPENDICES

A: OVERVIEW OF TIEMPO

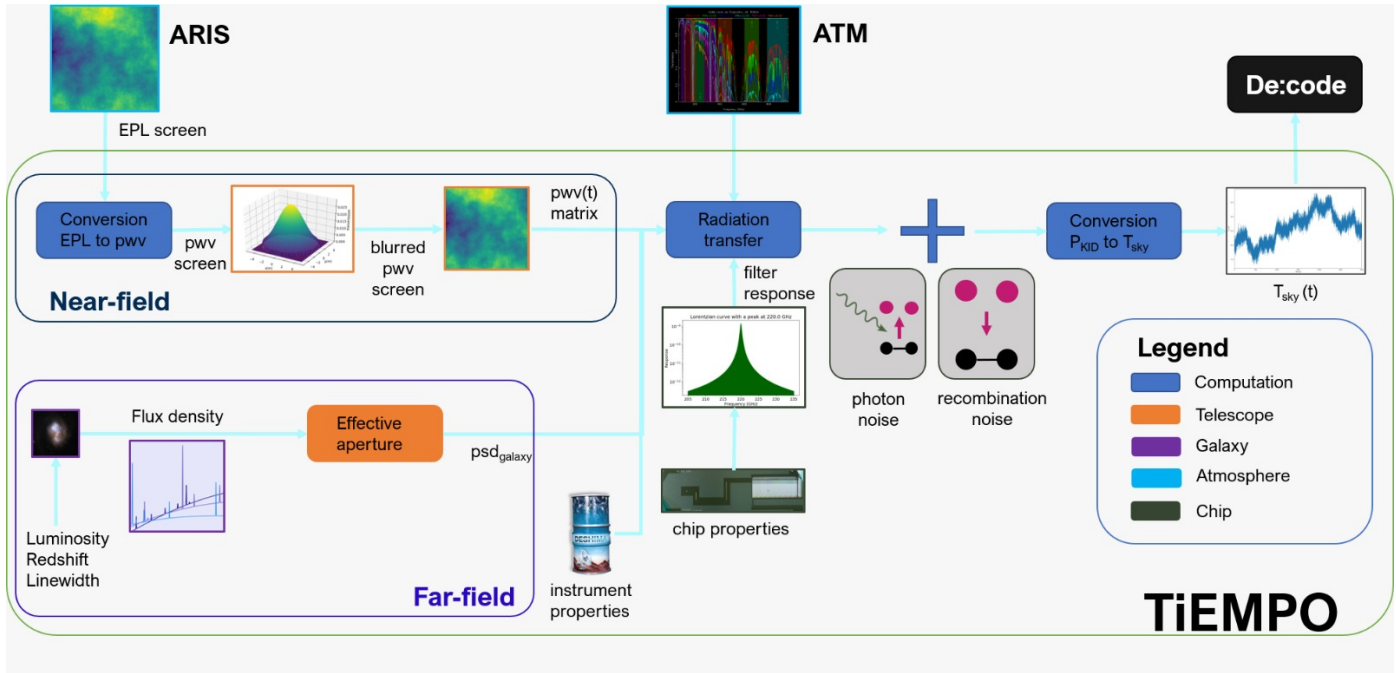


Figure A1: Complete overview of TIEMPO. Both internal and external section have been incorporated. Obtained from [1].

B: USED TIEMPO PARAMETERS

Table B1: An overview of the parameters that were used in the TiEMPO simulations in this thesis. In addition, the file in which the parameter is located is denoted. For certain files, the functions in which the variables should be changed are given in brackets.

Parameter	DESHIMA 1.0	DESHIMA 2.0
<i>main.py</i>		
F_min	$332 \cdot 10^9$	$220 \cdot 10^9$
num_bins	1500	1500
spec_res	300	500
num_filters	Use actual filter frequencies	Use actual filter frequencies
windspeed	10	10
beam_radius	5.	5.
useDESIM	1	1
inclAtmosphere	1	1
luminosity	<i>no galaxy</i>	<i>no galaxy</i> or 13.7
redshift	<i>no galaxy</i>	<i>no galaxy</i> or 4.43
linewidth	<i>no galaxy</i>	<i>no galaxy</i> or 600
EL	88.	60.
pwv_0	1.7	1.
D1	1	0
<i>use_desim.py (init)</i>		
eta_M1_spill	0.99	0.99
eta_M2_spill	0.90	0.90
n_wo_mirrors	2.	4.
window_AR	False	True
eta_co	0.65	0.65
eta_lens_antenna_rad	0.81	0.81
eta_circuit	$0.35 \cdot 0.1$	0.35
eta_IBF	0.6	0.6
KID_excess_noise_factor	1.0	1.1
Tb_cmb	2.725	2.725
Tp_amb	273.	273.
Tp_cabin	290.	290.
Tp_co	4.	4.
Tp_chip	0.12	0.12
<i>use_desim.py (transmit_through_DESHIMA, obt_data and calcT_psd_P methods)</i>		
theta_maj	$31.4 \cdot \text{np.pi}/180./60./60.$	<code>use_desim.D2HPBW(F_bins_Lor)</code>
theta_min	$22.8 \cdot \text{np.pi}/180./60./60.$	<code>use_desim.D2HPBW(F_bins_Lor)</code>
eta_mb	0.34	<code>self.eta_mb_ruze(F=F_bins_Lor, LFlimit=0.8, sigma=37e-6) \cdot 0.9</code>

Remark: When running either of the two simulations without a galaxy in it, only the *self.psd_gal* variable in the *transmit_signal_DESIM_multf_atm* function from the *signal_transmitter.py* file of TiEMPO has to be set to zero. All other parameters should be left unaltered.

C: TiEMPO DATA WITHOUT ADDED ATMOSPHERIC DRIFT

As indicated in Chapter 4.2.1, the addition of atmospheric drift to TiEMPO data appeared to give rise to some issues. In Figure C1, an illustration of the effect of adding the artificial atmospheric drift to the data from TiEMPO is given:

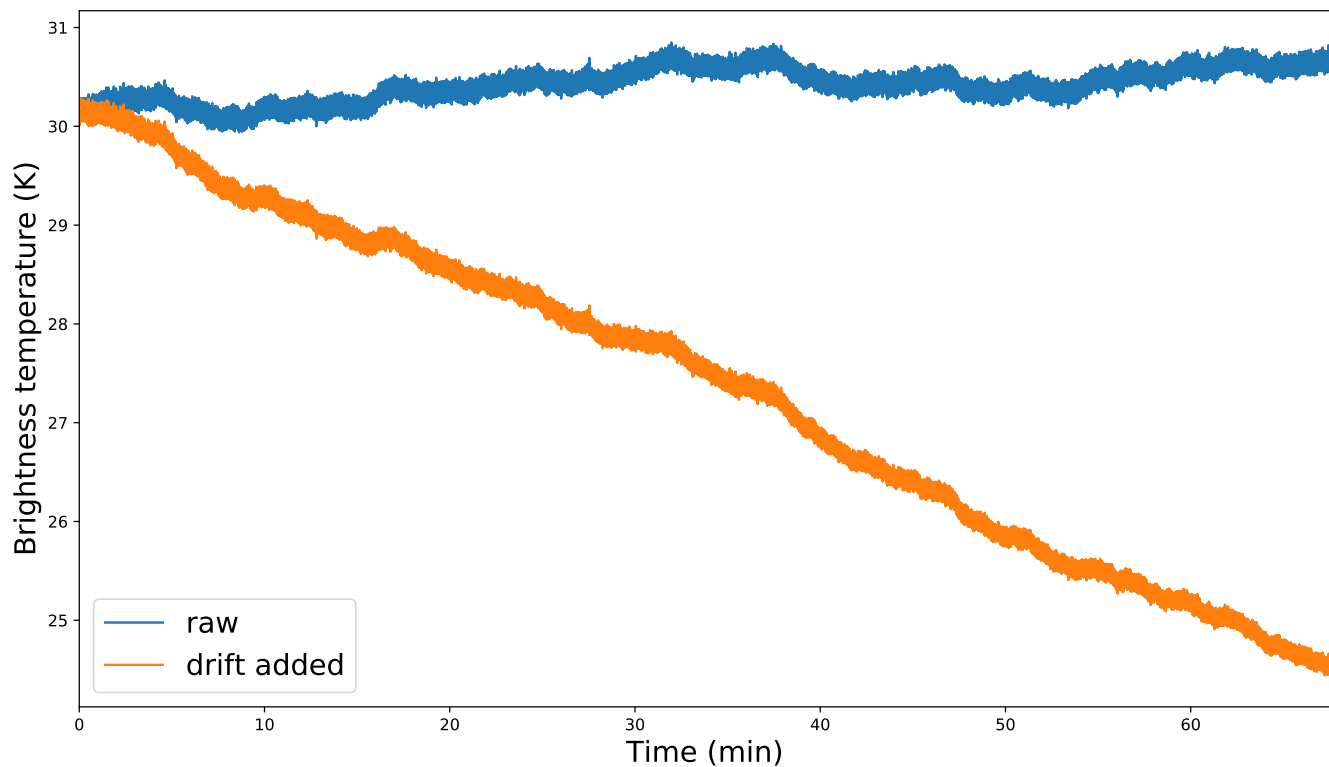


Figure C1: Plot of data acquired from TiEMPO before (blue) and after (orange) artificially adding an atmospheric drift to it. Besides the wanted drop in brightness temperature, the orange line also becomes narrower for longer observation times, which is incorrect.

As can be seen, not only the wanted drop in brightness temperature can be observed, but also the unwanted side effect of the orange line becoming narrower for longer observation times. This side-effect indicates that not only the atmospheric, but also the photon noise has been altered due to the drift addition, which is incorrect.

The effect of this faulty implementation can be spotted when Figure 4.4 is compared with Figure C2, which is plotted below.

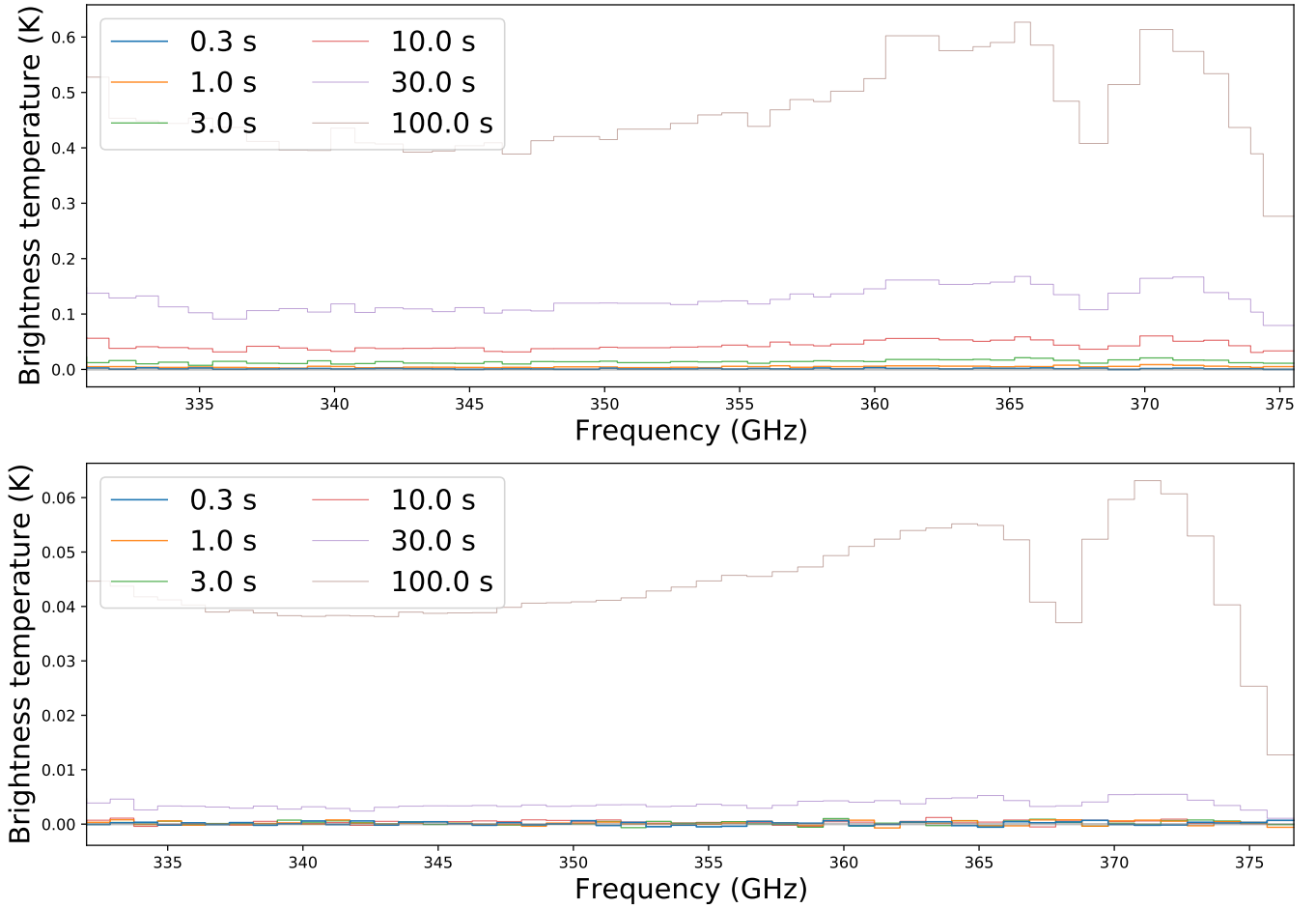


Figure C2: Plot very similar to that of Figure 4.4, but this time without an atmospheric drift added to it. The two plots in this image are much more similar in shape than the ones in Figure 4.4, but a difference in offset does appear. As this offset difference was not present in Figure 4.4, it is most likely caused by the absence of an atmospheric drop.

This comparison shows that, when the drift is not included in the OFF-OFF chopping strategy, the plots actually become very similar in shape. The downside is, however, that a difference in offset occurs for higher chopping frequencies. As this offset difference was not present in Figure 4.4, it is most likely caused by the absence of an atmospheric drift.

Despite the mismatch in shape and/or offset due to the faulty drift addition, the effect on the dynamical ABBA chopping seem to be relatively small. This can be seen when comparing the non-galaxy containing plots with and without an atmospheric drift (Figures 4.11 and C3) and when looking at the plots that do contain galaxy data, once again with and without an atmospheric drift (Figures 4.12 and C4).

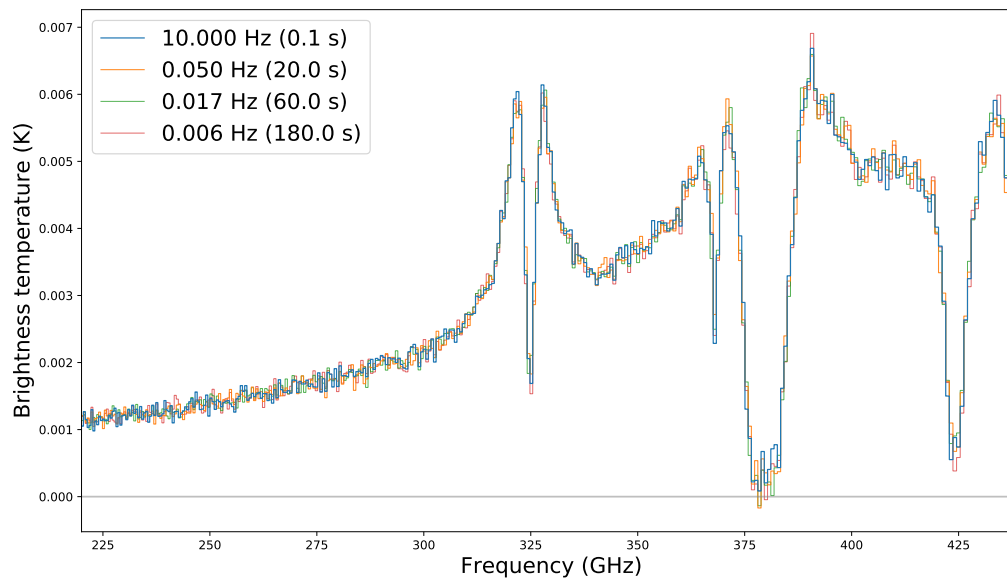


Figure C3: Just like in Figure 4.11, a dynamical ABBA chopping strategy is plotted. This time, however, the TiEMPO data has no atmospheric drift added to it.

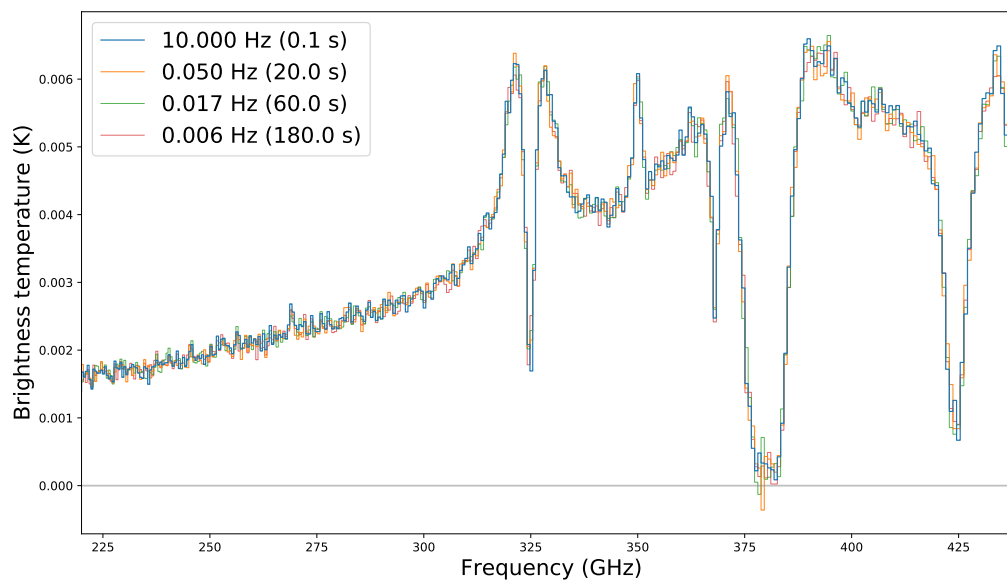


Figure C4: Like before, a plot similar to that in Figure 4.12, but without an atmospheric drift added to it.

These plots actually show great resemblance with their corresponding plots in Chapter 4.5 that do have a drift added to it. Only a slight difference in offset and peak values can be seen, which do not interfere with the galaxy detection method. This is again visualised when plotting the difference between the two spectra plotted in Figures C3 and C4, and comparing it with the corresponding plot in Figure 4.13:

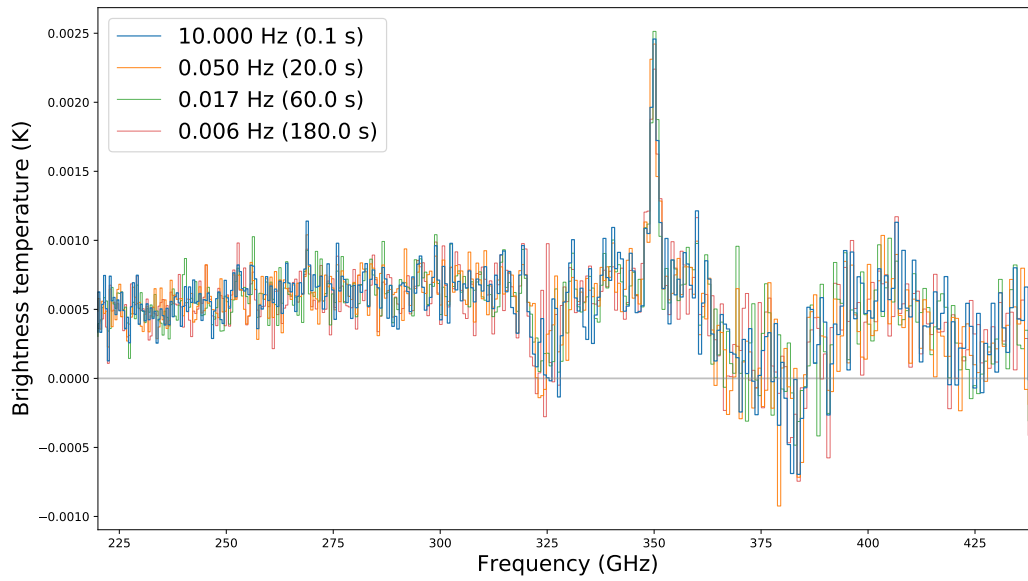


Figure C5: A plot of the difference between the plots in Figures C3 and C4. Comparing this plot with Figure 4.13 shows that the two have great resemblance in shape, with only a minor difference in the peak and offset values.

When comparing the figures in this section with those of Chapter 4.5, only a slight difference in offset and peak values can be seen. This indicates that, although heavily impacting the shape and offset of the OFF-OFF chopping strategy, the ABBA chopping method is not heavily affected by the faulty addition of the atmospheric noise. Therefore, the conclusions drawn in Chapter 4.5 can still be considered as reasonably accurate. For a more accurate and correct atmospheric addition, the drift has to be added before being processed by TiEMPO.

D: PROJECT OUTPUT

1. This BSc Thesis and the final presentation on 17-08-2020
2. The initialisation of the new Ubuntu server called *Galaxy*, which can be used for running Linux-based software. For this thesis, the galaxy observation simulations have been run via a Jupyter Notebook that was running on this new server.
3. The modelling and key results of the TiEMPO simulation program have been accepted as a poster presentation at the international conference SPIE Astronomical Telescopes + Instrumentation, San Diego, California, United States, 13-18 December 2020, as:

Modeling of the DESHIMA spectrometer for validating the software and calibration method
Esmee Huijten, Yannick Roelvink, Kaushal Marthi, Stan Zaalberg, Akio Taniguchi, Tom Bakx, Jochem J. A. Baselmans, Kah Wuy Chin, Robert Huiting, Kenichi Karatsu, Alejandro Pascual Laguna, Yoichi Tamura, Tatsuya Takekoshi, Stephen J. C. Yates, Maarten van Hoven, and Akira Endo

4. Several scripts for the used observation simulations, which can be used by others to continue the research performed for this report. These scripts include the algorithms for:
 - (a) Power Spectral Density calculation and comparison
 - (b) Noise-Equivalent Flux Density calculation and comparison
 - (c) Drift addition to existing TiEMPO data set
 - (d) ABBA chopping simulation (stationary and dynamical)
5. Some guides for using the Linux-based software created for this thesis can be found on the internal ASTRO workspace on Kibela:
 - (a) "Running DESHIMA Simulation 2.0 on Windows"
 - (b) "Running Deshima Simulation 2.0 on Galaxy server" (Still in process at time of writing)
6. Intermediate reports of performed research can be found on the internal DESHIMA workspace on Kibela:
 - (a) "Analysis of PWV data from ARIS"
 - (b) "50 vs. 1 um RMS PWV Analysis"
 - (c) "Time and PSD Analysis of noisy Tsky data"
 - (d) "DESHIMA 1 raw data vs model analysis"
 - (e) "Galaxy Observations using TiEMPO"
 - (f) "Updated ABBA Chopping Simulations of DESHIMA"

ACKNOWLEDGEMENTS

First of all, I would like to thank Akira Endo for his endless support during my Thesis. Even though we had to communicate predominantly via online communication tools due to the current Corona crisis, you were always there to help me and answer my questions regarding my project. During the relatively short time I was able to join you in your research, you taught me a lot about performing (astronomical) research, how to write scientifically correct and how to work in a team. In addition, your enthusiasm and optimism regarding my research have been a continuous source of motivation for me during my project.

In addition: Esmee Huijten, Akio Taniguchi, Jochem Baselmans, Tom Bakx, Kenichi Karatsu, Kaushal Marthi, Stephen Yates, Keiichi Matsuda, Yoichi Tamura and Tatsuya Takekoshi, thank you all for listening to my midway updates and providing me with your professional feedback. Because of your sharp criticism my research has concluded the way it did, providing a most interesting prospect for future DESHIMA research. Furthermore, I would like to give my special thanks to Stephen Yates and Aurèle Adam, for the time and effort they put into forming the Thesis committee for this report.

Moreover, I would like to thank the Experimental Astronomy group as a whole. Even though the Corona times have prevented me from working alongside you guys in Delft, I always felt very accepted and involved within the group. It was very interesting to see how researchers from various different scientific backgrounds were able to work together as smoothly and joyfully as all of you did.

Last but not least, I would like to thank my family, my friends and my girlfriend for providing me their support and suggestions throughout my project I would also like to give a special thanks to Sylvie and Christian Tarrade, for taking me into their house during the French national lockdown and for caring for both me and Manon for its duration.

BIBLIOGRAPHY

- [1] E. Huijten, *TiEMPO: Time-Dependent End-to-End Model for Post-process Optimization of the DESHIMA Spectrometer*, Bachelor's thesis, Delft University of Technology (2020), <https://repository.tudelft.nl/islandora/object/uuid:5302e10e-3b56-4d4d-a1fd-6a1d58f57abd?collection=education>.
- [2] C. M. Casey, D. Narayanan, and A. Cooray, *Dusty Star-Forming Galaxies at High Redshift*, *Physics Reports* **541**, 45 (2014), arXiv: 1402.1456.
- [3] R. S. Asano, T. T. Takeuchi, H. Hirashita, and A. K. Inoue, *Dust formation history of galaxies: A critical role of metallicity* for the dust mass growth by accreting materials in the interstellar medium*, *Earth, Planets and Space* **65**, 11 (2013).
- [4] A. Endo, K. Karatsu, Y. Tamura, T. Oshima, A. Taniguchi, T. Takekoshi, S. Asayama, T. J. L. C. Bakx, S. Bosma, J. Bueno, K. W. Chin, Y. Fujii, K. Fujita, R. Huiting, S. Ikarashi, T. Ishida, S. Ishii, R. Kawabe, T. M. Klapwijk, K. Kohno, A. Kouchi, N. Llombart, J. Maekawa, V. Murugesan, S. Nakatsubo, M. Naruse, K. Ohtawara, A. Pascual Laguna, J. Suzuki, K. Suzuki, D. J. Thoen, T. Tsukagoshi, T. Ueda, P. J. de Visser, P. P. van der Werf, S. J. C. Yates, Y. Yoshimura, O. Yurduseven, and J. J. A. Baselmans, *First light demonstration of the integrated superconducting spectrometer*, *Nature Astronomy* **3**, 989 (2019).
- [5] T. Takekoshi, K. Karatsu, J. Suzuki, Y. Tamura, T. Oshima, A. Taniguchi, S. Asayama, T. J. L. C. Bakx, J. J. A. Baselmans, S. Bosma, J. Bueno, K. W. Chin, Y. Fujii, K. Fujita, R. Huiting, S. Ikarashi, T. Ishida, S. Ishii, R. Kawabe, T. M. Klapwijk, K. Kohno, A. Kouchi, N. Llombart, J. Maekawa, V. Murugesan, S. Nakatsubo, M. Naruse, K. Ohtawara, A. Pascual Laguna, K. Suzuki, D. J. Thoen, T. Tsukagoshi, T. Ueda, P. J. de Visser, P. P. van der Werf, S. J. C. Yates, Y. Yoshimura, O. Yurduseven, and A. Endo, *DESHIMA on ASTE: On-Sky Responsivity Calibration of the Integrated Superconducting Spectrometer*, *Journal of Low Temperature Physics* **199**, 231 (2020).
- [6] A. Endo, P. d. Visser, and J. Baselmans, *Course Presentation for EE4635 Superconducting Astronomical Instrumentation*, TU Delft (2020).
- [7] J. Huchra, *Extragalactic Redshifts*, <http://ned.ipac.caltech.edu/help/zdef.html>.
- [8] G. J. Stacey, *Thz low resolution spectroscopy for astronomy*, *IEEE Transactions on Terahertz Science and Technology* **1**, 241 (2011).
- [9] G. B. Rybicki and A. P. Lightman, *Radiative Processes in Astrophysics* (1986).
- [10] J. Cernicharo, *Atm: a program to compute atmospheric transmission between 0-1000 ghz*, Internal Rep. Institut de Radioastronomie Millimétrique (IRAM) (1985).
- [11] Almascience, *Atmosphere model*, <https://almascience.eso.org/about-alma/atmosphere-model>.
- [12] A. Thompson, J. Moran, and G. Swenson Jr, *Interferometry and Synthesis in Radio Astronomy* (Astronomy and Astrophysics Library, 2017).
- [13] Y. Asaki, H. Sudou, Y. Kono, A. Doi, R. Dodson, N. Pradel, Y. Murata, N. Mochizuki, P. G. Edwards, T. Sasao, *et al.*, *Verification of the effectiveness of vsop-2 phase referencing with a newly developed simulation tool, aris*, *Publications of the Astronomical Society of Japan* **59**, 397 (2007).
- [14] Y. Asaki, M. Saito, R. Kawabe, K.-i. Morita, Y. Tamura, and B. Vila-Vilaro, *Alma memo no. 535 simulation series of a phase calibration scheme with water vapor radiometers for the atacama compact array*, NRAO (2005).

- [15] Y. Sewnarain Sukul, *Principal component analysis on atmospheric noise measured with an integrated superconducting spectrometer*, Bachelor's thesis, Delft University of Technology (2019), <http://resolver.tudelft.nl/uuid:a75fde14-e7fb-401c-9c47-2f954fc5e70c>.
- [16] A. Taniguchi and T. Ishida, *De:code*, (2020), <https://github.com/deshima-dev/decode>.
- [17] T. Wilson, K. Rohlf, and S. Huettemeister, *Tools of Radio Astronomy*, 5th ed., Astronomy and Astrophysics Library (Springer-Verlag, Berlin Heidelberg, 2009).
- [18] C. M. Van vliet and G. S. Kousik, *Noise in Physical Systems and 1/f Noise*, edited by A. D'amico and P. Mazzetti (Elsevier, Amsterdam, 1986) pp. 3 – 10.
- [19] K. Marthi, *Modelling kinetic inductance detectors and associated noise sources*, Industrial Internship Project Report (University of Groningen and SRON, 2020) <http://fse.studenttheses.ub.rug.nl/id/eprint/23044>.
- [20] A. Pascual Laguna, K. Karatsu, A. Neto, A. Endo, and J. J. A. Baselmans, *Wideband Sub-mm Wave Superconducting Integrated Filter-bank Spectrometer*, in *2019 44th International Conference on Infrared, Millimeter, and Terahertz Waves (IRMMW-THz)* (IEEE, Paris, France, 2019) pp. 1–2.
- [21] D. J. Benford, T. R. Hunter, and T. G. Phillips, *Noise Equivalent Power of Background Limited Thermal Detectors at Submillimeter Wavelengths*, *International Journal of Infrared and Millimeter Waves* **19**, 931 (1998).
- [22] W. Feller, *An introduction to probability theory and its applications* (New York, Wiley, 1957).
- [23] A. Endo and A. Taniguchi, *Deshima-sensitivity*, <https://github.com/deshima-dev/deshima-sensitivity> (2020).
- [24] K. Volk, *Chopping and Nodding for Mid-Infrared Astronomy*, (2007).